Immune landscapes predict chemotherapy resistance and immunotherapy response in acute myeloid leukemia

Jayakumar Vadakekolathu[1], Mark D. Minden[2], Tressa Hood[3], Sarah E. Church[3], Stephen Reeder[1], Heidi Altmann[4], Amy H. Sullivan[3], Elena J. Viboch[3], Tasleema Patel[5], Narmin Ibrahimova[2], Sarah E. Warren[3], Andrea Arruda[2], Yan Liang[3], Thomas H. Smith[3], Gemma A. Foulds[1], Michael D. Bailey[3], James Gowen-MacDonald[3], John Muth[6], Marc Schmitz[7,8,9], Alessandra Cesano[3], A. Graham Pockley[1,10], Peter J.M. Valk[11], Bob Löwenberg[11], Martin Bornhäuser[4,8,9], Sarah K. Tasian[5], Michael P. Rettig[12], Jan Davidson-Moncada[6], John F. DiPersio[12], Sergio Rutella[1,10,*]

[1]John van Geest Cancer Research Centre, Nottingham Trent University, Nottingham, NG11 8NS, United Kingdom
[2]Division of Medical Oncology and Hematology, Princess Margaret Cancer Centre, Toronto, ON M5G 2C1, Canada
[3]NanoString Technologies Inc., Seattle, WA 98109, United States of America
[4]Department of Medicine, Universitätsklinikum Carl Gustav Carus, 01307 Dresden, Germany
[5]Department of Pediatrics, Division of Oncology and Centre for Childhood Cancer Research, Children's Hospital of Philadelphia and University of Pennsylvania School of Medicine, PA 19104, United States of America
[6]MacroGenics Inc., Rockville, MD 20850, United States of America
[7]Institute of Immunology, Faculty of Medicine Carl Gustav Carus, Technische Universität Dresden, 01307 Dresden, Germany
[8]National Center for Tumor Diseases (NCT), Partner Site Dresden, 01307 Dresden, Germany
[9]German Cancer Consortium (DKTK), Partner Site Dresden, and German Cancer Research Center (DKFZ), 69120 Heidelberg, Germany
[10]Centre for Health, Ageing and Understanding Disease (CHAUD), Nottingham Trent University, Nottingham, NG11 8NS, United Kingdom
[11]Department of Hematology, Erasmus University Medical Centre, 3000CA Rotterdam, Netherlands
[12]Division of Oncology, Department of Internal Medicine, Washington University in St. Louis, St. Louis, MO 63110, United States of America

*To whom correspondence should be addressed:
E-mail: sergio.rutella@ntu.ac.uk
Open Researcher and Contributor Identifier (ORCID) ID: 0000-0003-1970-7375

One Sentence Summary: Dissecting the immune architecture of AML and its influence on therapeutic response identifies patients for whom immunotherapy will be most beneficial.

Abstract: Acute myeloid leukemia (AML) is a molecularly and clinically heterogeneous hematological malignancy. Although immunotherapy may be an attractive modality to exploit in patients with AML, the ability to predict the groups of patients and the types of cancer that will respond to immune targeting remains limited. This study dissected the complexity of the immune architecture of AML at high resolution and assessed its influence on therapeutic response. Using 442 primary bone marrow samples from three independent cohorts of children and adults with AML, we defined immune-infiltrated and immune-depleted disease classes and revealed critical differences in immune gene expression across age groups and molecular disease subtypes. Importantly, interferon (IFN)-γ-related mRNA profiles were predictive for both chemotherapy resistance and response of primary refractory/relapsed AML to flotetuzumab immunotherapy. Our compendium of microenvironmental gene and protein profiles provides insights into the immuno-biology of AML and could inform the delivery of personalized immunotherapies to IFN-γ-dominant AML subtypes.

Introduction

Acute myeloid leukemia (AML) is a malignant disorder characterized by the accumulation of myeloblasts in the bone marrow (BM) and blood (*1*). The discovery of the genomic landscape of AML, including the identification of targetable mutations (*2*), has propelled the development of novel anti-leukemic agents and is enabling disease classification and patient stratification into risk groups (*3*). Despite success in many areas, AML is cured in only 35-40% of patients <60 years of age and in 5-15% of patients >60 years of age. While chemotherapy resistance is common, the majority of patients die of disease relapse. Investigation of new molecularly-targeted and immuno-modulatory agents therefore remains a high priority for both children and adults (*4*).

Tumor phenotypes are dictated not only by the neoplastic cell component, but also by the immunologic milieu within the tumor microenvironment (TME), which is equipped to subvert host immune responses and hamper effector T-cell function (*5*). *In silico* approaches have been instrumental for the identification of immunogenomic features with therapeutic and prognostic implications. In solid tumors, six immune subtypes have been described: wound healing, interferon (IFN)-γ-dominant, inflammatory, lymphocyte-depleted, immunologically quiet, and transforming growth factor (TGF)-β-dominant (*6*). These are characterized by differences in macrophage or lymphocyte signatures, T helper type (Th)-1 to Th2 cell ratio, extent of intratumoral heterogeneity and neoantigen load, aneuploidy, cell proliferation, expression of immunomodulatory genes, and patient survival (*6*).

Although immunotherapy may be an attractive modality to exploit in patients with AML (*7*), the ability to predict the groups of patients and the forms of leukemia that will respond to immune targeting remains limited (*8-11*). Clinical studies in patients with solid tumors have shown that responses to anti-programmed cell death 1 (PD-1)/programmed death ligand 1 (PD-L1)-targeted immunotherapy occur most often in individuals with immune-inflamed lesions that are characterized by pre-existing CD8^{+} T-cell responses, release of pro-inflammatory and effector cytokines (*12-14*), and an augmented T-cell receptor (TCR) clonal diversity pre-treatment (*15,*

16). The T-cell inflamed gene expression profile (GEP) is a measure of IFN-γ-responsive genes that are related to adaptive immune resistance (AIR) mechanisms of immune escape such as indoleamine 2,3-dioxygenase-1 (*IDO1*) and *PD-L1* (*17*), and is predictive of clinical benefit with pembrolizumab immunotherapy (*18, 19*). Although IFN-γ plays a critical role in eliciting anti-tumor T-cell activity and enabling tumor rejection, prolonged IFN-γ signaling under conditions of persistent antigen exposure has been shown to activate a PD-L1-independent, STAT1-driven multigenic program which confers resistance to radiotherapy and anti-cytotoxic T-lymphocyte antigen 4 (CTLA-4) immunotherapy in mouse models of melanoma (*20*).

Herein, we used targeted immune gene expression profiling (IGEP) and spatially resolved multiplexed digital spatial profiling (DSP) for the high-dimensional analysis of the immunological contexture of a broad collection of BM samples from patients with AML and for the identification of molecular determinants of immunotherapeutic benefit. We reveal unifying immune features and critical differences that define classes and subclasses of TMEs and deliver predictions of chemotherapy resistance, survival and immunotherapy response that are beyond the current capabilities of single molecular markers.

Results

Targeted immune gene expression profiling (IGEP) identifies immune subtypes of AML

We first analyzed unfractionated, archival BM samples from treatment-naïve patients with non-promyelocytic AML (PMCC discovery series; n=290 cases; **Table 1**) (*21*). We derived immune scores from mRNA expression, similar to those of previous publications, and devised an RNA-based, quantitative metric of immune infiltration (*22, 23*). As shown in **Fig. S1A-B**, patients with adverse cytogenetic features exhibited a shorter relapse-free survival (RFS) and overall survival (OS) compared with patients with intermediate and favorable cytogenetic risk, thus confirming the overall performance of well-established European Leukemia-Net (ELN) categories (*24*). A Pearson correlation matrix of immune gene sets allowed us to identify co-expression patterns of pre-defined immune cell types and immune biological activities. Immune signature modules in pre-treatment BM samples reflected the co-expression of genes associated with 1) type I and type II IFN biology, 2) adaptive immune responses, and 3) myeloid cell abundance (macrophages, neutrophils and dendritic cells [DCs]); **Fig. 1A**). We then computed the sum of the individual scores in each signature module in **Fig. 1A** and generated three immune scores (IFN-dominant, adaptive, and myeloid) which individually separated AML cases according to high and low expression values (**Fig. S1C**). Specifically, the IFN-dominant gene module was calculated as the sum of IFN-γ signaling, IFN downstream, immunoproteasome, myeloid inflammation, inflammatory chemokine, *IL-10*, MAGEs, *PD-L1* and *PD-L2* scores. When considered in aggregate, IFN-dominant, adaptive, and myeloid scores dichotomized BM samples into two immune subtypes, herein termed immune-infiltrated and immune-depleted (**Fig. 1B** and **Fig. S1D-E**) (*25*), which expressed comparable amounts of leukemia-associated antigens CD34, CD123 (*IL3RA*) and CD117 (*KIT*). This observation suggests that targeted IGEP of bulk BM specimens largely captured elements of the immunological TME rather than features of the tumor cell compartment (**Fig. S1F**).

As shown in **Fig. 1C**, AML cases with immune-infiltrated profiles had higher expression of IFN-stimulated genes and T-cell recruiting factors (*STAT1*, *CXCL10*, *IRF1*), T-cell markers and

cytolytic effectors (*CD8A*, *CD8B*, *GZMB*, *PRF1*), counter-regulatory immune checkpoints and immunotherapy drug targets (*IDO1*, *CTLA4*, *PD-L1* and *BTLA*), and molecules involved in antigen processing and presentation (*TAP1*, *TAP2*, *HLA-A*, *HLA-B* and *HLA-C*). Conceivably, high T-cell infiltration and expression of MHC and PD-L1 in the immune-infiltrated AML subtype reflected a pre-existing IFN-γ-driven adaptive immune response. This type of response has previously been associated with suppressed anti-tumor immune reactivity (*13, 26*), but also with immunotherapy responses in patients with solid tumors (*9, 18, 27*) and AML (*11*). *STAT1*, a central component of the IFN-γ signaling pathway and predictor of response to immune checkpoint blockade (*28*), was more strongly correlated with the presence of T-cell inhibitory receptors *TNFRSF14* (a ligand for the immunoglobulin superfamily members BTLA and CD160), *PD-L1*, *HAVCR2* (Tim-3) and *LAG-3*, and with IFN-stimulated genes *MX1*, *IFIT1* and *IRF1* in the immune-infiltrated relative to the immune-depleted subtype, consistent with their coordinated regulation in an inflamed TME (**Fig. 1D**).

Highly multiplexed digital spatial profiling (DSP) reveals distinct T-cell neighbors in immune-infiltrated and immune-depleted AML

Transcriptomic data do not provide information on spatial relationships of tumor-infiltrating immune cells within the TME. Therefore, we used GeoMx DSP to characterize the expression of 31 immuno-oncology (IO) proteins in 10 randomly selected, fresh frozen paraffin embedded (FFPE) BM biopsies from treatment-naïve patients with AML (SAL cohort) with varying degrees of T-cell infiltration (**Fig. S2** and **Fig. S3**). We selected 24 geometric regions of interest (ROIs) per BM sample using fluorescent anti-CD3 (visualization marker for T-cell-rich ROIs) and anti-CD123 antibodies (visualization marker for myeloid blast-rich ROIs; **Fig. 2A**) (*29*). T-cell gene expression scores (calculated as detailed in **Fig. S4A**) correlated with DSP CD3 protein status (**Fig. S4B**). Furthermore, mRNA and proteins for B cells (P = 0.0026), monocytes (P = 0.0156) and Bcl-2 (P = 0.0139) significantly and positively correlated, serving as a validation for the mRNA-based immune scores (**Fig. S4C**).

We then asked whether CD3-rich and CD3-poor BM samples (defined by a median split of barcode counts) differed in terms of co-localization patterns of relevant IO proteins. As shown in **Fig. S4D**, CD3+ T-cells in immune-infiltrated biopsies co-localized with B cells, antigen processing and presentation-related proteins (β2-microglobulin), negative immune checkpoint B7-H3 and β-catenin. In contrast, CD3+ T-cells in immune-depleted biopsies co-localized with markers of immunological memory (CD45RO) and T-cell exhaustion (PD-1). We next assigned each ROI to either the T-cell-rich (CD3 "hotspot") or the T-cell-poor category, using the top and bottom quartile of CD3 barcode counts (**Fig. S5A**). When compared to T-cell-poor ROIs, CD3 hotspots showed higher protein expression of CD8, β2-microglobulin, B7-H3, PD1, total and phosphorylated STAT3, CD14 and CD19 (**Fig. S5B**). As shown in **Fig. 2B**, PTEN positively correlated with CD8 and GZMB. Furthermore, baseline expression of PD-L1, Bcl-2, VISTA, Ki-67 and FoxP3 was significantly lower in patients who achieved remission in response to induction chemotherapy compared to patients with primary induction failure (**Fig. S5C**).

When analyzing overall protein expression patterns (10 samples × 24 ROIs *per* sample × 31 proteins = 7,440 data points), we identified four protein signatures (SIG), which were then further assessed *in silico* for correlations with clinical-biological disease characteristics and potential prognostic value in The Cancer Genome Atlas (TCGA)-AML cases (162 sequenced AML samples with putative copy-number alterations, mutations and mRNA expression *z*-scores [threshold±2.0]). Abnormalities in SIG1, SIG2 and SIG4 genes (blue boxes in **Fig. 2C**) did not correlate with specific disease characteristics or clinical outcomes. In contrast, mRNA up-regulation, gene amplification, deep deletion and mis-sense mutations in SIG3 genes, which were detected in 26% of TCGA-AML cases as mutually exclusive genomic events (**Fig. 2D**), significantly correlated with *TP53* mutation status, an established adverse prognosticator in AML (*P* value from mutation enrichment analysis=0.0285). SIG3 were enriched for gene ontology (GO) biological processes related to T-cell lineage commitment, positive T-cell selection and T-cell homeostasis (**Fig. 2E**). De-regulation in SIG3 genes, which included *PD-*

L1, *FoxP3*, *GZMB*, *PTEN* and *BCL2*, were predominantly observed in patients with immune-infiltrated mRNA profiles (**Fig. 2F**) and correlated with higher number of mutations ($P = 0.021$) and with adverse ELN cytogenetic features ($\chi^2=25.03$; $P < 0.001$), but not with other disease characteristics at presentation, including white blood cell (WBC) count, and percentage of AML blasts in pre-treatment blood and BM samples. Finally, patients with abnormalities in SIG3 genes experienced poor clinical outcomes, as shown by the significantly lower RFS and OS rates (**Fig. 2G**). Although the mutually exclusive pattern of SIG3 genomic abnormalities would suggest that the altered genes are linked in a common biological process or pathway (*30*), *GZMB* and *FoxP3* were the only SIG3 genes that individually predicted shorter OS (**Fig. S6**). Collectively, highly multiplexed *in situ* detection of IO proteins highlights critical differences in T-cell infiltrated *versus* T-cell depleted AML subtypes and identifies protein signatures with prognostic potential in T-cell infiltrated pre-treatment samples.

Interactions between immune subgroups, common cytogenetic alterations and clinical factors
We next correlated immune signature scores with clinical and demographic factors, including WBC count and blast cell count at diagnosis, ELN cytogenetic category (available in 249 cases from the PMCC discovery series) and patient age. Leukemia burden was significantly lower in the immune-infiltrated AML subtype (median WBC count at diagnosis $P < 0.0001$; median percentage of BM blasts $P < 0.0001$; and median number of AML blasts per μL of blood $P < 0.0001$; **Fig. S7A-C**). Immune signature scores were not correlated with the ELN cytogenetic risk category when considered individually (**Fig. S7D**). Finally, patients with high immune infiltration tended to be of a more advanced age at diagnosis compared with patients with low immune infiltration ($P < 0.0001$; **Fig. S7E**).

Immune subtypes improve survival prediction
The activation of immune pathways has context-dependent prognostic impact that differs between tumor types (*6*). We next assessed the ability of the immune subtype to refine the

accuracy of outcome prediction separately for each ELN cytogenetic risk category. Among patients with favorable risk, RFS and OS times were significantly longer in individuals with an immune-infiltrated TME (**Fig. 3A**). In contrast, clinical outcomes in ELN adverse risk cases were worse in individuals with an immune-infiltrated TME (**Fig. 3A**). Interestingly, CD8 exhaustion scores and PD1 scores were significantly higher in patients with ELN adverse risk compared with ELN favorable risk (**Fig. 3B**), suggesting that leukemia progression may be sustained by tumor cell-extrinsic (immune) mechanisms in patients with more aggressive disease. We also observed that the ELN classifier assisted outcome prediction only in the immune-infiltrated subtype (**Fig. 3C**), allowing the identification of patient subgroups with excellent survival estimates (87.5% RFS and 77.8% OS) or with very unsatisfactory outcomes [10.4% RFS (log-rank χ^2=15.07; P < 0.0001) and 7.2% OS (log-rank χ^2=25.75; P < 0.0001)]. Unexpectedly, our immunological classifier was unable to stratify survival in patients with intermediate ELN risk. ELN intermediate patients with *NPM1* mutation and *FLT3*-ITD information (available in 100 cases) were then subclassified into molecular low risk (*NPM1* mutations without *FLT3*-ITD), molecular intermediate risk (*NPM1* wild-type without *FLT3*-ITD or with low *FLT3*-ITD allelic ratio) and molecular high risk cases (*NPM1* wild-type with high *FLT3*-ITD allelic ratio) (*31*). As shown in **Fig. 3D**, the molecular classifier separated survival both in patients with immune-infiltrated AML and in those with an immune-depleted TME. The inclusion of immune gene signatures also improved the ability of *NPM1* and *FLT3*-ITD mutation status to predict survival in multivariate logistic regression models relative to molecular risk alone (AUROC=0.938 *versus* 0.765; **Fig. 3E**). Specifically, the IFN downstream score (Wald χ^2=4.1; P = 0.043), CD8 score (Wald χ^2=4.2; P = 0.04), exhausted CD8$^+$ T-cell score (Wald χ^2=4.4; P = 0.037), *IDO1* score (Wald χ^2=4.01; P = 0.045) and *CTLA4* score (Wald χ^2=5.2; P = 0.022) significantly contributed to the model.

By performing Cox proportional hazards regression, we also discovered a set of 21 differentially expressed (DE) immune genes [false discovery rate (FDR)<0.05] between the favorable and adverse-risk ELN category (**Fig. 4A** and **Table S1**). This gene set was highly

expressed in immune-infiltrated AMLs (**Fig. 4B**) and separated ELN intermediate patients into subgroups with low and high gene expression values, with the former being closely similar to ELN favorable-risk patients while the latter resembled ELN adverse-risk patients. The 21-gene classifier exhibited enrichment of gene ontologies (GO) and pathways related to T-cell activation, TCR downstream signaling and regulation of cytokine production (**Fig. 4C**). Importantly, RFS and OS estimates were significantly worse for intermediate-risk patients with high *versus* low expression of the 21 DE genes (**Fig. 4D**). This finding was validated *in silico* using transcriptomic data from two independent AML cohorts (TCGA [**Fig. 4E**] and HOVON [**Fig. 4F**]).

Finally, we used informative censoring to evaluate the impact of the immune subtypes on outcome whilst excluding potential clinical benefit from graft-versus-leukemia (GVL) effects after allogeneic HSCT. As shown in **Fig. S8A** and compared to all patients, survival differences remained evident when patients were censored on the date of allogeneic HSCT, suggesting that immune gene profiles largely predicted outcome after conventional chemotherapy. A competing risks regression analysis in which allogeneic HSCT was treated as a potential confounder (*32, 33*) confirmed that the IFN-dominant gene module, but not the adaptive and myeloid gene modules, predicted for shorter OS (**Table S2**). We also assessed the potential impact of the immune subtype on post-transplantation outcomes. Causes of death were not different in patients with immune-infiltrated and immune-depleted AML (**Table S3**). In contrast to patients with immune-depleted AML, individuals with immune-infiltrated AML benefited from a more profound GVL effect after allogeneic HSCT, as suggested by a significantly longer median OS time (31.9 months) compared with patients receiving chemotherapy only (18.9 months, log-rank P = 0.018). Patients with immune-infiltrated AML and adverse ELN features derived the greatest benefit from allogeneic HSCT (28% *versus* 3% survival rate after chemotherapy with or without allogeneic HSCT, respectively; **Fig. S8B-C**).

Immune landscapes stratify AML patients in independent validation sets and differ across age groups and disease stages

AML is a disease with age-dependent biological specificities (*34, 35*). Furthermore, pediatric AML are inherently of low immunogenicity and are therefore less likely to respond to single-agent checkpoint inhibition (*36*). To characterize the immunological landscape of AML across age groups and longitudinally in patients who initially achieve complete remission (CR) and then experience disease recurrence, we profiled BM samples from a pediatric (CHOP series, n=34 cases, 61 BM specimens in total) and an adult AML cohort (SAL series, n=46 cases, 91 BM specimens in total). In line with findings in the PMCC discovery series, we identified IFN-dominant, adaptive and myeloid mRNA profiles (**Fig. S9A-D**) which individually separated AML cases according to high and low expression values and, when considered in aggregate, dichotomized AML cases into an immune-infiltrated and immune-depleted subtype (**Fig. S9E-F**). As summarized in **Fig. 5A**, comparison between children and adults with AML revealed a set of DE immune genes involved with cytokine and chemokine signaling, as indicated by GO (**Fig. S10A** and **Table S4**) and protein interaction network analysis (**Fig. S10B**). Specifically, genes encoding pro-inflammatory and pro-angiogenic cytokines and chemokines, including *IL8*, *CCL3L1*, *CCL3* and *CXCL2*, were more expressed in adult AML relative to childhood AML (**Fig. 5A**). The tumor inflammation signature (TIS) score and the IFN-γ score were significantly higher in elderly patients (>60 years of age) relative to younger adults (<60 years of age) and to children aged less that 18 years (**Fig. S10C**).

When comparing matched BM samples from a subset of adult patients in the SAL series (n=21) at the time of diagnosis and achievement of CR after induction chemotherapy (**Fig. 5B** and **Fig. S11**), we identified a set of DE genes that were enriched for GO biological processes related to immune responses, apoptosis, drug resistance, transcriptional mis-regulation, and cell surface receptor/cytokine-mediated signaling (**Table S5**). As shown in **Fig. 5B**, *FLT3*, *CD99*, and milk-fat globule EGF-8 (*MGFE8)*, which have previously been implicated in cancer stem cell self-renewal (*37*), were lower in AML cases with CR, serving as a data reliability check. In agreement with recently published observations (*38*), *CTLA4* expression was higher in CR relative to disease onset, with concomitant down-regulation of *CD244* coinhibitory molecule, suggesting the occurrence of T-cell activation after treatment (**Fig. S10D**).

Furthermore, immune genes significantly associated with relapsed AML (SAL series) largely captured CD8$^+$ T-cell infiltration, elements of T-cell biology, including TCR downstream signaling (*CD8A*, *CD5*, *CD3z [CD247]*), leukocyte differentiation and immune regulation (**Fig. 5C** and **Table S6**). The increased expression of surrogate markers of terminal T-cell differentiation, senescence and exhaustion [*TBX21* (T-bet) (*39, 40*), *TIGIT*, *KLRD1* (*38*) and *KLRF1*] in relapsed AML suggests that BM-infiltrating cytotoxic T cells may fail to restrain leukemia growth (**Fig. S10E**). The DE genes between patient subgroups with newly diagnosed, CR and relapsed AML in the SAL cohort, and between childhood and adult cases, were largely non-overlapping, as shown in **Fig. 5D**.

Upon activation with a polyclonal stimulus, intracellular cytokine staining of BM suspensions showed higher concomitant production of IFN-γ and TNF-α by microenvironmental CD4$^+$ and CD8$^+$ T lymphocytes in the immune-infiltrated compared with the immune-depleted subgroup (*P* = 0.0273; **Fig. S12A-D**). Polyfunctional IFN-γ^+TNF-α^+ T cells were significantly reduced in remissional BM samples compared with diagnostic and relapse BMs (*P* = 0.0257) and were particularly low in patients with documented minimal residual disease (MRD) negativity (**Fig. S12E**).

IFN-related gene sets improve the prediction of therapy resistance

We then asked whether the IFN-dominant gene module may assist the prediction of therapeutic resistance, which we empirically defined as failure to achieve CR in patients who survived at least 28 days (primary refractory AML) or as early relapse (<3 months) after achieving CR, as previously published by others (*41*). When patients in the PMCC cohort were dichotomized based on higher or lower than median IFN scores, a higher percentage of patients with primary refractory disease was observed in the IFN-score^{high} AML cases (65.4% *versus* 34.6%; *P* = 0.0022, Fisher's exact test), suggesting that transcriptional programs orchestrated by microenvironmental IFN-γ might render AML blasts resistant to chemotherapeutic agents (*20, 42*). In contrast, the frequency of primary refractory cases was

not different when comparing patients with higher or lower than median adaptive module scores (29.6% *versus* 25.4%; *P* = NS) and myeloid module scores (26.7% *versus* 28.1%; *P* = NS). In multivariate logistic regression analysis, the IFN-related module scores improved the ability of the ELN category to predict therapeutic resistance, but not patient survival (**Fig. 6A-B**; **Table S7**). Specifically, the myeloid inflammation score (*P* = 0.003), IFN-γ signaling score (*P* = 0.014) and IFN downstream score (*P* = 0.034) significantly contributed to the model (**Table S7**). Gene sets defining gene modules 2 and 3 in **Fig. 1**, reflective of adaptive immune responses and BM infiltration with cells of the myeloid lineage, respectively, were not associated with either therapeutic resistance or patient survival.

We next tested the predictive and prognostic power of immune scores *in silico* using a broad collection of public transcriptomic data. We initially devised binary logistic regression models utilizing RNA-sequencing data from 196 patients on the Beat AML Master Trial with clinical response information (*43*). When considering disease type (primary *versus* secondary), WBC count and patient age at diagnosis, the inclusion of genes capturing IFN-γ-related biology significantly improved the predictive ability of the ELN risk category (AUROC=0.921 *versus* 0.709 with ELN cytogenetic risk alone; model χ^2=106.4 *versus* 29.6; increased specificity=4%; increased sensitivity=17%; decreased false positive rate=39%; decreased false negative rate=18%; **Fig. 6C**).

Confirming our findings in the PMCC and Beat AML cohorts, IFN-dominant, adaptive and myeloid mRNA profiles, when used in aggregate, stratified patients in the HOVON database (618 non-promyelocytic AML cases (*44*)) into subgroups with high and low immune infiltration (**Fig. 6D-E**). Individuals with immune-infiltrated AML had lower leukemia burden (median percentage of BM blasts=56% *versus* 71% in patients with immune-depleted AML; *P* < 0.0001) and tended to have more advanced age at diagnosis (median=51 years, range 15-74, *versus* 46 years, range 15-77; *P* = 0.0067). A higher percentage of patients with IFN-dominant AML failed to achieve CR in response to induction chemotherapy when compared to non-IFN-dominant AML cases (27.2% *versus* 15.2%; *P* = 0.0004, Fisher's exact test). In contrast, the

occurrence of primary induction failure was not different when patients were dichotomized based on higher or lower than median adaptive module scores (21.4% *versus* 21.0% IF rate; P = NS) or myeloid module scores (21.7% *versus* 20.7% IF rate; P = NS). Gene set enrichment analysis (GSEA) with all transcripts in the HOVON dataset provided as input and ranked by the $\log_2$ fold-change between non-responders and responders confirmed the over-expression of curated hallmark gene sets linked to IFN-γ responses and inflammatory responses in chemotherapy-refractory patients (**Fig. 6F**). When tested in a multinomial logistic regression model incorporating patient age, leukemia burden and ELN cytogenetic risk (available in 615 HOVON cases) (*45*), immune gene sets defining the IFN-dominant module significantly and independently predicted whether patients responded to induction chemotherapy and whether they experienced disease relapse (**Table S8**). In contrast, immune gene signatures were unable to assist the prediction of non-leukemic deaths (**Table S8**).

Mutations in tumor suppressor genes and transcription factors are enriched in immune-infiltrated AML cases

It has recently been shown that genetic drivers of solid malignancies dictate neutrophil and T-cell recruitment, thus affecting the immune milieu of the tumor and assisting patient stratification (*46*). We asked whether clonal driver mutations may correlate with the immune subtypes that we identified herein. We therefore retrieved TCGA AML RNA-sequencing data from cBioPortal (http://www.cbioportal.org/) and computed immune cell type-specific and biological activity scores (*22*). IFN-related gene sets, including the TIS score, were higher in TCGA-AML cases with *TP53* and *RUNX1* mutations relative to molecular lesions that confer favorable or intermediate risk (**Fig. S13A**). In contrast, the majority of TCGA-AML cases with *NPM1* mutations with or without *FLT3*-ITD (intermediate-risk and favorable-risk cases, respectively) were classified as immune-depleted. Clonal hematopoiesis of indeterminate potential (CHIP) is a hematological malignancy precursor condition defined by somatic mutations in leukemia-associated driver genes, including *DNMT3A*, *TET2* and *ASXL1*, and associated with increased risk for inflammatory diseases of aging (*47*). Interestingly, the TIS

score, but not the IFN-γ score, was significantly higher in TCGA AML cases with CHIP-defining mutations compared with patient subgroups with other molecular lesions (**Fig. S13B**). When extending our *in-silico* analysis to the Beat AML cohort (281 cases in total), 16 out of 17 (94%) *TP53*-mutated AMLs expressed higher amounts of genes implicated in downstream IFN signaling and higher *CD8* transcripts and markers of cytotoxicity compared with *TP53* wild-type cases (**Fig. S14A-B**).

IFN-γ-related gene expression and protein profiles correlate with anti-leukemia responses after flotetuzumab immunotherapy

Finally, we hypothesized that higher expression of IFN-γ-related genes in immune-infiltrated AML cases, while underpinning chemotherapy resistance, might identify patients with AML who derive benefit from immunotherapy with flotetuzumab (*48*), a CD3×CD123 dual affinity re-targeting (DART) molecule. BM samples collected prior to flotetuzumab treatment from 30 adult patients with chemotherapy-refractory or relapsed AML enrolled in the CP-MGD006-01 clinical trial (NCT#02152956) were profiled using the PanCancer IO360 gene expression assay. Patients' characteristics are summarized in **Table S9** and flotetuzumab anti-leukemic activity was defined as either CR, CR with partial hematologic recovery (CRh), CR with incomplete hematologic recovery (CRi), partial response or overall benefit (>30% reduction in BM and/or blood blasts). BM samples from 92% of patients with evidence of flotetuzumab anti-leukemic activity (11 out of 12) had an immune-infiltrated TME relative to non-responders (**Fig. 7A**). The IFN-dominant module score was significantly higher in patients with chemotherapy-refractory AML compared with relapsed AML at time of flotetuzumab treatment, and in individuals with evidence of anti-leukemic activity compared to non-responders (**Fig. 7B**). Notably, the TIS score was a strong predictor of anti-leukemic responses to flotetuzumab, with an AUROC value of 0.847 (**Fig. 7C**). On-treatment BM samples (available in 19 patients at the end of cycle 1) displayed increased antigen presentation and immune activation relative to baseline samples, as reflected by higher TIS scores (6.47±0.22 *versus* 5.93±0.15, *P* =

0.0006), antigen processing machinery scores (5.67±0.16 *versus* 5.31±0.12, *P* = 0.002), IFN-γ signaling scores (3.58±0.27 *versus* 2.81±0.24, *P* = 0.0004) and *PD-L1* expression (3.43±0.28 *versus* 2.73±0.21, *P* = 0.0062; **Fig. 7D**). GeoMx DSP of BM FFPE biopsies from a subgroup of 11 patients identified protein profiles at baseline that distinguish responders from non-responders (**Fig. 7E-F** and **Fig. S15**). The IFN-γ-inducible molecule STING was upregulated post-cycle 1 of flotetuzumab in two patients who achieved CR (**Fig. 7G**). In these individuals, T-cell activation markers (CD27, CD45RO, CD44), Bcl-2, immune checkpoints (ICOS, PD-L2, CTLA4 and 4-1BB [CD137]) and CD4 were highly expressed in ROIs with T-cell clustering (CD3 hotspots) around CD123+ AML blasts (**Fig. 7H**), supporting a local immune-modulatory effect of flotetuzumab. Overall, these data suggest a clinical benefit for AML patients with an immune-infiltrated TME and validate the translational relevance of our findings.

Discussion

Using large cohorts of subjects, the current study reveals underlying transcriptomic features that stratify the TME of AML into immune subtypes and may assist therapeutic predictions by defining patients who will potentially derive the greatest benefit from immunotherapies. We identified two subtypes of differentially immune-infiltrated tumors, an observation that was validated in independent childhood and adult AML series, reinforcing the notion that unique molecular features can distinguish AML across age groups (*35*). The IFN-related gene sets identified in our study improved the prediction of therapeutic resistance following conventional '3+7' cytarabine and anthracycline chemotherapy beyond that provided by the ELN cytogenetic risk category (AUC=0.815 in PMCC cases [discovery series] and 0.870 in Beat AML cases [*in silico* validation series]) (*49*). In recent Southwestern Oncology Group (SWOG) and MD Anderson Cancer Center clinical trials, pretreatment covariates such as cytogenetic risk and age only yielded AUROCs of 0.65 and 0.59 for therapeutic resistance, respectively (*41*). Models that were established in the present study by incorporating IFN-related mRNA profiles also outperform a recently developed 29-gene and cytogenetic risk predictor of chemotherapy resistance (AUROC=0.76) (*50*). Our observation that CD8 exhaustion scores and PD1 scores are significantly higher in patients with ELN adverse risk compared with ELN favorable risk is congruent with a previous report showing unique transcriptional programs associated with ELN cytogenetic risk groups in CD8$^+$ T cells from patients with AML (*51*). Intriguingly, an IFN-related DNA damage resistance signature (IRDS) correlates with resistance to adjuvant chemotherapy and with recurrence after radiotherapy in patients with breast cancer (*42*), suggesting that tumor cells over-expressing IRDS genes, including *STAT1*, *ISG15* and *IFIT1*, as a result of chronic activation of the IFN signaling pathway might receive pro-survival rather than cytotoxic signals in response to DNA damage (*52*).

The immune-infiltrated AML cases were highly immune-suppressed, as indicated by elevated expression of IFN-inducible negative immune checkpoints and immunotherapy targets *IDO1* and *PD-L1*, and simultaneously secreted high amounts of IFN-γ and TNF-α, a measure of polyfunctional Th1 responses (*53*). Furthermore, adults with relapsed AML in the SAL series

expressed a higher magnitude of T-cell exhaustion molecules relative to matched pre-treatment samples, suggesting the occurrence of escape from immune surveillance at the time of disease relapse (*54*). In general, solid tumors with a substantial T-cell component and displaying a type I immune response are associated with better OS and progression-free survival estimates (*6*). However, the highly proliferative IFN-γ-dominant solid tumors may correlate with a less favorable survival, despite being infiltrated with CD8$^+$ T cells and harboring the highest type 1 macrophage signature scores (*6*). By utilizing targeted IGEP, our study highlights that the activation of IFN-related pathways and the relative abundance of immune cell types, including the over-expression of T-cell markers and TCR signaling intermediates in relapsed AML relative to disease onset, have negative prognostic implications in AML. This is conceivably the result of a non-productive anti-leukemia immune response and/or IFN-driven resistance to DNA damage induced by chemotherapeutic agents (*20*). Patients with immune-infiltrated AML at baseline had better OS estimates when treated with allogeneic HSCT compared with chemotherapy alone, suggesting that GVL effects were more profound in this patient subgroup. In contrast, no survival advantage from allogeneic HSCT was evident in patients with immune-depleted AML.

The heterogeneity of immune infiltration can also be determined by tumor cell-intrinsic factors, including chemokine secretion (*55*) and expression of cancer driver genes, all of which affect response to immunotherapies (*46, 56, 57*). Interestingly, we detected associations between mutations in tumor suppressor and cancer driver genes and immune subtypes of AML and we identified *TP53* mutations as being strongly correlated with an IFN-γ-dominant TME and with prognostic protein signatures, including the expression of PD-L1, FOXP3, PTEN and GZMB, that were revealed by spatially-resolved, highly multiplexed protein profiling. Notably, GZMB expression has recently been associated with features of exhaustion and senescence in AML CD8$^+$ T cells (*38*). A recent study showed higher proportions of PD-L1-expressing CD8$^+$ T cells, activation of IFN-γ-associated genes and favorable responses to pembrolizumab immunotherapy in *TP53*-mutated lung cancers (*58*). It is tempting to speculate that immune-

infiltrated, *TP53*-mutated AML cases, which have very low response rates when treated with standard anthracycline-based and cytarabine-based induction chemotherapy, could benefit from T cell-targeting approaches and/or hypomethylating agents that potentially alter the immune surveillance of AML (*59*). PTEN loss has been correlated with reduced CD8$^+$ T-cell infiltration, with lower expression of *IFNG* and *GZMB* transcripts and with resistance to immune checkpoint blockade in metastatic melanoma and in primary sarcoma (*60, 61*). The higher expression of CD8 and GZMB that we observed in ROIs with higher PTEN suggests that PTEN may represent a novel molecular driver of T-cell infiltration in AML. In addition, higher expression of GZMB correlated with worse clinical outcomes and individually separated AML patients into subgroups with different survival probabilities. In this respect, signatures of dysfunctional T cells, including high expression of *GZMB* and other transcripts associated with effector CD8$^+$ T-cell differentiation such as *IFNG*, may be increased in AML patients at diagnosis and persist with higher frequency only in chemotherapy non-responders (*38*). Finally, IFN-γ-related gene expression programs in the AML TME, including the TIS score, correlated with response to flotetuzumab immunotherapy in 30 heavily pre-treated patients with relapsed/refractory AML on clinical trial CP-MGD006-01. Flotetuzumab treatment was associated with increased expression of antigen processing machinery components, IFN-γ signaling molecules such as STING, negative immune checkpoints and lymphocyte activation markers, including heightened *PD-L1* mRNA and protein, in BM ROIs with CD3 hotspots. This finding provides a biological rationale for designing clinical studies with sequential flotetuzumab and immune checkpoint blockade in AML patients in remission with minimal residual disease.

The use of bulk BM aspirates is a potential limitation of our analysis. Future studies should use single-cell RNA sequencing of purified CD8$^+$ T cells to further dissect individual variation in response to T-cell engagers (*62*). We also acknowledge that the detailed phenotypes, antigen specificities and intratumoral TCR repertoires of T cells in patients with immune-infiltrated AML remain to be established (*63*).

In conclusion, our work unveils the heterogeneity of the immune landscape of AML and provides a novel precision medicine-based conceptual framework for delivering T cell-targeting immunotherapy to subgroups of patients with IFN-γ-dominant AML, who may be refractory to conventional cytotoxic chemotherapy but responsive to T-cell engagers. The immunological stratification of pre-treatment BM samples may therefore enable rapid risk prediction and selection of frontline therapeutic modalities (*11*), in conjunction with cytogenetic and mutational information.

Materials and Methods

Study design

The CP-MGD006-01 clinical trial (NCT#02152956) is a multicenter, open-label, phase 1/2 dose escalation and dose expansion study. Thirty patients with primary refractory (n=23) and relapsed AML (n=7) treated with flotetuzumab at the recommended phase 2 dose (500 ng/kg/day) were included in the current analysis. Patients received a lead-in dose of flotetuzumab during week 1, followed by 500 ng/kg/day during weeks 2-4 of cycle 1, and a 4-day on/3-day off schedule for cycle 2 and beyond. Eligible patients were 18 years of age or older, with relapsed or refractory AML (according to WHO criteria) unlikely to benefit from cytotoxic chemotherapy defined as a) refractory to ≥ 2 induction attempts (primary induction failure); b) first relapse with an initial complete remission (CR) duration < 6 months (early relapse) or relapse in patients that achieve a CR lasting ≥ 6 months following prior therapy (late relapse), or d) prior failure of hypomethylating agents. All participants were required to have Eastern Cooperative Oncology Group performance status of ≤ 2, a peripheral blast count of < 20,000/mm^3 at the time of first treatment, and adequate organ function. Patients with a prior history of allogeneic HSCT, active untreated autoimmune disorders, or active central nervous system leukemia were excluded. The trial was approved by the Institutional Review Boards of participating centers and was conducted according to the current International Conference on Harmonization (ICH) Guideline for Good Clinical Practice (ICH E6), and all applicable local and national regulations and ethical principles in accordance with the Helsinki Declaration. All participants provided written informed consent prior to enrollment.

BM aspirates were collected at baseline (n=30) and after cycle 1 of flotetuzumab (n=19) to evaluate the temporal immunological effects associated with therapeutic response. Disease status was assessed by modified IWG criteria. Anti-leukemic response was defined as either CR, CR with incomplete hematologic recovery (CRi), CR with partial hematologic recovery (CRh), partial remission (PR) or "other benefit" (OB; >30% decrease in BM blasts). Non-responders were individuals with either treatment failure (TF), stable disease (SD) or progressive disease (PD). Patient and disease characteristics are detailed in **Table S8**.

Patients' demographics (discovery cohorts)

Patient and disease characteristics are detailed in **Table 1**. Primary patient specimens (non-promyelocytic AML) and associated clinical data were obtained on research protocols approved by the Investigational Review Boards of the Children's Hospital of Philadelphia (CHOP), USA and Princess Margaret Cancer Centre (PMCC), Canada and by the Ethics Committee of TU Dresden and Studienallianz Leukämie (SAL), Germany.

RNA isolation and processing

Messenger RNA was isolated and processed as previously described (*45*). For the PMCC, SAL and CHOP patient cohorts, 100-150 ng per sample of RNA extracted from 442 bulk BM aspirates from patients with AML treated with curative intent were analyzed on the NanoString nCounter FLEX analysis system using the PanCancer Immune [PCI] profiling panel (for research use only and not for use in diagnostic procedures), which measures mRNA expression of 770 genes representing 14 immune cell types, common checkpoint inhibitors, cancer testis antigens and genes covering both the innate and adaptive immune response without the need for amplification (*25, 64, 65*). BM samples from patients receiving flotetuzumab immunotherapy were analyzed using the PanCancer IO 360 panel (for research use only and not for use in diagnostic procedures).

nCounter data quality control, data normalization and signature calculation

The reporter probe counts, i.e., the number of times the color-coded barcode for that gene is detected, were tabulated in a comma separated value (CSV) format for data analysis with the nSolver software package (version 4.0.62) and nSolver Advanced Analysis module (version 2.0.115; NanoString Technologies). The captured transcript counts were normalized to the geometric mean of the housekeeping reference genes included in the assay and the code set's internal positive controls. The relative abundance of immune cell types and immuno-oncology biological signatures were computed as previously published (*22, 23*). For samples

run on the PCI profiling panel, we also calculated an approximation of the TIS using 16 of the 18 functional genes and 5 of the 10 housekeeper genes that are present in the PanCancer IO360 mRNA panel (*18*).

Gene ontology (GO) and gene set enrichment analysis (GSEA)

Metascape.org was used to enrich genes for GO biological processes and pathways. GSEA was performed using the GSEA software v.3.0 (Broad Institute, Cambridge, USA) (*66*). The hallmark IFN-γ response (M5911) and inflammatory response gene sets (M5913) were downloaded from the Molecular Signature Database (MSigDB) (*22, 23*).

GeoMx Digital Spatial Profiling (DSP)

Ten FFPE BM biopsies from patients with newly diagnosed AML (SAL series) and 19 FFPE BM biopsies from patients receiving flotetuzumab immunotherapy (n=11 at baseline and n=8 post-cycle 1) were profiled using the prototype or commercial GeoMx DSP platform, respectively (**Fig. S15**). Samples were stained using 3 fluorescent visualization markers, CD3 (T cell), CD123 (myeloid blast), SYTO 83 or 13 (nuclei), and UV-cleavable oligo-labeled antibodies (panels are shown in **Table S10**). Stained slides were loaded on the DSP instrument and digitally scanned. Fluorescent scans were used to select 24 geometric regions of interest (ROIs) for molecular profiling (*27, 67*). The DSP instrument then UV-illuminated selected ROIs to release conjugated oligos and the micro-capillary fluidics system collected released oligos, which were counted on the nCounter system. Data were normalized to technical controls and area.

Intracellular cytokine staining

Cells were aliquoted into 12×75mm tubes ($0.5×10^6$ cells per tube) in 500 μL RPMI1640 (Lonza) + 10% fetal bovine serum (FBS) (v/v). Two tubes were set up per sample, the first as an unstimulated control and the second stimulated with 50 ng/mL PMA and 1 μg/mL ionomycin (both from Sigma Aldrich). Samples also received 10 μg/mL brefeldin A (BioLegend), then were vortexed gently and incubated at 37°C for 5 hours. Following incubation, cells were

washed in PBS then incubated in 100 μL PBS containing 5 μL Human FcR Blocking Reagent (Miltenyi Biotec), fluorescently labeled mAbs for surface markers of interest (CD3, CD4, CD8; BioLegend) and fixable LIVE/DEAD viability stain (Molecular Probes) for 30 minutes at 4°C protected from light. Unbound antibody was washed off using PBS, then cells were fixed by incubating in 200 μL 1×True-Nuclear Fix Buffer (True-Nuclear Transcription Factor Buffer Set, BioLegend) for 20 minutes. Cells were washed in 1×Perm Buffer (True-Nuclear Transcription Factor Buffer Set, BioLegend) then resuspended in 100 μL 1×Perm Buffer and fluorescently-labeled mAbs for intracellular cytokines of interest (IL-2, IL-4, IL-10, IL-17, IFN-γ and TNF-α; antibody clones are provided in **Table S11**) and incubated for 20 minutes at room temperature protected from light. Unbound antibody was washed off using 1×Perm Buffer, cells were resuspended in 400 μL PBS and immediately analyzed on a 3-laser, 10-color Gallios flow cytometer (Beckman Coulter).

Data sources for in silico analyses

The first data series (E-MTAB-3444), hereafter referred to as the HOVON series (*44*), was retrieved from Array Express and encompassed three independent cohorts of adults (≤60 years) with *de novo* AML (last accessed on March 4, 2019). BM and blood samples were collected at diagnosis and were analyzed on the Affymetrix Human Genome U133 Plus 2.0 Microarray (*44, 68*). Patients were treated with curative intent according to the Dutch-Belgian Hematology-Oncology Cooperative Group and the Swiss Group for Clinical Cancer Research (HOVON/SAKK) AML-04, -04A, -29, -32, -42, -42A, -43 or -92 protocols (available at http://www.hovon.nl). Clinical annotations were provided by the authors. The second data series, hereafter referred to as The Cancer Genome Atlas (TCGA) series, consisted of RNA-sequencing data (Illumina HiSeq2000) from 162 adult AML patients with complete cytogenetic, immunophenotypic and clinical annotation who were enrolled on Cancer and Leukemia Group B (CALGB) treatment protocols 8525, 8923, 9621, 9720, 10201 and 19808 (*69*). RNA and clinical data were retrieved from the TCGA data portal (https://tcga-data.nci.nih.gov/tcga/tcgaDownload.jsp). The third data series (Beat AML) was retrieved using

the VIZOME user interface (http://www.vizome.org/aml/) and consisted of RNA-sequencing data from primary specimens from 281 AML patients with detailed clinical annotations, including diagnostic information, treatments, responses and outcomes treated on the Beat AML Master Trial (*43*). Patient and disease characteristics for *in silico* data sources are summarized in **Data File S1**.

Statistical analyses

Descriptive statistics included calculation of mean, median, SD, and proportions to summarize study outcomes. Comparisons were performed with the Mann-Whitney *U* test for paired or unpaired data (two-sided), as appropriate, or with the ANOVA with correction for multiple comparisons. IBM SPSS Statistics (version 24) and GraphPad Prism (version 8) were used for statistical analyses. A two-sided *P* value < 0.05 was considered to reflect statistically significant differences. The log-rank (Mantel-Cox) test was used to compare survival distributions.

Therapeutic resistance was defined as failure to achieve complete remission (CR) despite not experiencing early treatment-related mortality (within 28 days of chemotherapy initiation; primary refractory cases) or as early relapse (<3 months) after achieving CR (*41*). Overall survival (OS) was computed from the date of diagnosis to the date of death. Relapse-free survival (RFS) was measured from the date of first CR to the date of relapse or death. Subjects lost to follow-up were censored at their date of last known contact.

Binary logistic regression and multinomial logistic regression were used to ascertain the relative contribution of immune subtypes and other pretreatment covariates selected *a priori* based on known clinical relevance (ELN risk group, *FLT3*-ITD status, *NPM1* mutational status, patient age at diagnosis and primary *versus* secondary AML) toward the predicted likelihood of response to induction chemotherapy, AML relapse and patient death (*45*). Competing risks regression analyses by the method of Fine and Gray were performed using STATA/IC (version 16.0) (*32*). Allogeneic HSCT, a potential confounder, was treated as an event whose occurrence precluded the occurrence of the primary clinical endpoint (death) (*32*).

Supplementary Materials

Fig. S1. Immune gene signatures and survival in the AML discovery series (PMCC cohort; n=290 cases).

Fig. S2: GeoMx digital spatial profiling (DSP) and region of interest (ROI) selection in a representative pre-treatment BM trephine biopsy (SAL series) with high T-cell infiltration.

Fig. S3: GeoMx digital spatial profiling (DSP) and region of interest (ROI) selection in a representative pre-treatment BM trephine biopsy (SAL series) with low T-cell infiltration.

Fig. S4: Highly multiplexed protein profiling in the SAL patient cohort.

Fig. S5: Correlation between CD3 infiltration and expression of immuno-oncology (IO)-related proteins as revealed by GeoMx digital spatial profiling (DSP) of BM trephine biopsies (SAL series).

Fig. S6: Expression of SIG3 genes in TCGA-AML cases and in healthy tissues.

Fig. S7: Association between immune gene signatures and patients' characteristics in the AML discovery series (PMCC cohort; n=290 cases).

Fig. S8: Clinical outcomes of patients with immune-infiltrated and immune-depleted AML treated with allogeneic HSCT (PMCC cohort).

Fig. S9: Immune gene signatures in the CHOP and SAL cohorts.

Fig. S10: Gene ontology and pathway analyses.

Fig. S11: Immune scores in AML patients (SAL cohort) at time of diagnosis and achievement of complete remission (paired samples).

Fig. S12: Intracellular cytokine staining of BM samples from patients with immune-infiltrated and immune-depleted AML.

Fig. S13: Immune subtypes associate with cancer driver gene mutations in The Cancer Genome Atlas (TCGA)-AML and Beat AML trial specimens.

Fig. S14: Immune signature scores and cancer driver gene mutations in The Cancer Genome Atlas (TCGA)-AML and Beat AML trial specimens.

Fig. S15: Selection of regions of interest in BM biopsies from patients receiving flotetuzumab immunotherapy.

Table S1: Differentially expressed (DE) genes (false discovery rate<0.05) between ELN favorable-risk and adverse-risk AML (HOVON discovery cohort).

Table S2: Competing risks analysis for overall survival (OS) prediction (PMCC discovery cohort).

Table S3: Causes of death in patients receiving allogeneic hematopoietic stem cell transplantation (HSCT; PMCC cohort).

Table S4: Gene ontologies (GO) of and KEGG pathways captured by DE genes between adult (SAL cohort) and childhood AML (CHOP cohort).

Table S5: GO of and KEGG pathways captured by DE genes between adult AML patients at the time of diagnosis and achievement of complete remission (SAL cohort).

Table S6: GO of and KEGG pathways captured by DE genes between adult AML patients at the time of relapse and achievement of complete remission (SAL cohort).

Table S7: Binary logistic regression predicting therapeutic resistance (PMCC cohort).

Table S8: Multinomial logistic regression predicting therapeutic response (HOVON cohort).

Table S9: Study participants in the CP-MGD006-01 clinical trial (NCT#02152956) of flotetuzumab immunotherapy.

Table S10: Protein panels used for GeoMx Digital Spatial Profiling (DSP) of FFPE bone marrow biopsies (SAL cohort [A] and flotetuzumab cohort [B]).

Table S11: Antibody panel used for intracellular cytokine staining of bone marrow cell suspensions.

Data File S1: Patient and disease characteristics (*in silico* data sources).

References

1. H. Dohner, D. J. Weisdorf, C. D. Bloomfield, Acute myeloid leukemia. *N Engl J Med* **373**, 1136-1152 (2015).
2. E. Papaemmanuil, M. Gerstung, L. Bullinger, V. I. Gaidzik, P. Paschka, N. D. Roberts, N. E. Potter, M. Heuser, F. Thol, N. Bolli, G. Gundem, P. Van Loo, I. Martincorena, P. Ganly, L. Mudie, S. McLaren, S. O'Meara, K. Raine, D. R. Jones, J. W. Teague, A. P. Butler, M. F. Greaves, A. Ganser, K. Dohner, R. F. Schlenk, H. Dohner, P. J. Campbell, Genomic classification and prognosis in acute myeloid leukemia. *N Engl J Med* **374**, 2209-2221 (2016).
3. A. Khwaja, M. Bjorkholm, R. E. Gale, R. L. Levine, C. T. Jordan, G. Ehninger, C. D. Bloomfield, E. Estey, A. Burnett, J. J. Cornelissen, D. A. Scheinberg, D. Bouscary, D. C. Linch, Acute myeloid leukaemia. *Nat Rev Dis Primers* **2**, 16010 (2016).
4. C. C. Coombs, M. S. Tallman, R. L. Levine, Molecular therapy for acute myeloid leukaemia. *Nat Rev Clin Oncol* **13**, 305-318 (2016).
5. M. Binnewies, E. W. Roberts, K. Kersten, V. Chan, D. F. Fearon, M. Merad, L. M. Coussens, D. I. Gabrilovich, S. Ostrand-Rosenberg, C. C. Hedrick, R. H. Vonderheide, M. J. Pittet, R. K. Jain, W. Zou, T. K. Howcroft, E. C. Woodhouse, R. A. Weinberg, M. F. Krummel, Understanding the tumor immune microenvironment (TIME) for effective therapy. *Nat Med* **24**, 541-550 (2018).
6. V. Thorsson, D. L. Gibbs, S. D. Brown, D. Wolf, D. S. Bortone, T. H. Ou Yang, E. Porta-Pardo, G. F. Gao, C. L. Plaisier, J. A. Eddy, E. Ziv, A. C. Culhane, E. O. Paull, I. K. A. Sivakumar, A. J. Gentles, R. Malhotra, F. Farshidfar, A. Colaprico, J. S. Parker, L. E. Mose, N. S. Vo, J. Liu, Y. Liu, J. Rader, V. Dhankani, S. M. Reynolds, R. Bowlby, A. Califano, A. D. Cherniack, D. Anastassiou, D. Bedognetti, A. Rao, K. Chen, A. Krasnitz, H. Hu, T. M. Malta, H. Noushmehr, C. S. Pedamallu, S. Bullman, A. I. Ojesina, A. Lamb, W. Zhou, H. Shen, T. K. Choueiri, J. N. Weinstein, J. Guinney, J. Saltz, R. A. Holt, C. E. Rabkin, N. Cancer Genome Atlas Research, A. J. Lazar, J. S. Serody, E. G. Demicco, M. L. Disis, B. G. Vincent, L. Shmulevich, The immune landscape of cancer. *Immunity* **48**, 812-830 (2018).
7. S. Gill, S. K. Tasian, M. Ruella, O. Shestova, Y. Li, D. L. Porter, M. Carroll, G. Danet-Desnoyers, J. Scholler, S. A. Grupp, C. H. June, M. Kalos, Preclinical targeting of human acute myeloid leukemia and myeloablation using chimeric antigen receptor-modified T cells. *Blood* **123**, 2343-2354 (2014).
8. G. T. Gibney, L. M. Weiner, M. B. Atkins, Predictive biomarkers for checkpoint inhibitor-based immunotherapy. *Lancet Oncol* **17**, e542-e551 (2016).
9. R. Cristescu, R. Mogg, M. Ayers, A. Albright, E. Murphy, J. Yearley, X. Sher, X. Q. Liu, H. Lu, M. Nebozhyn, C. Zhang, J. K. Lunceford, A. Joe, J. Cheng, A. L. Webber, N. Ibrahim, E. R. Plimack, P. A. Ott, T. Y. Seiwert, A. Ribas, T. K. McClanahan, J. E. Tomassini, A. Loboda, D. Kaufman, Pan-tumor genomic biomarkers for PD-1 checkpoint blockade-based immunotherapy. *Science* **362**, (2018).
10. N. Daver, G. Garcia-Manero, S. Basu, P. C. Boddu, M. Alfayez, J. E. Cortes, M. Konopleva, F. Ravandi-Kashani, E. Jabbour, T. Kadia, G. M. Nogueras-Gonzalez, J. Ning, N. Pemmaraju, C. D. DiNardo, M. Andreeff, S. A. Pierce, T. Gordon, S. M. Kornblau, W. Flores, Z. Alhamal, C. Bueso-Ramos, J. L. Jorgensen, K. P. Patel, J. Blando, J. P. Allison, P. Sharma, H. Kantarjian, Efficacy, safety, and biomarkers of response to azacitidine and nivolumab in relapsed/refractory acute myeloid leukemia: A nonrandomized, open-label, phase II study. *Cancer Discov* **9**, 370-383 (2019).
11. S. Rutella, S. E. Church, J. Vadakekolathu, E. Viboch, A. H. Sullivan, T. Hood, S. E. Warren, A. Cesano, R. La Motte-Mohs, J. Muth, H. Lelièvre, B. Lowenberg, J. F. DiPersio, J. K. Davidson-Moncada, Adaptive immune gene signatures correlate with response to flotetuzumab, a CD123 × CD3 bispecific DART® molecule, in patients with relapsed/refractory acute myeloid leukemia. *Blood* **132**, 444-444 (2018).
12. D. S. Chen, I. Mellman, Elements of cancer immunity and the cancer-immune set point. *Nature* **541**, 321-330 (2017).

13. P. C. Tumeh, C. L. Harview, J. H. Yearley, I. P. Shintaku, E. J. Taylor, L. Robert, B. Chmielowski, M. Spasic, G. Henry, V. Ciobanu, A. N. West, M. Carmona, C. Kivork, E. Seja, G. Cherry, A. J. Gutierrez, T. R. Grogan, C. Mateus, G. Tomasic, J. A. Glaspy, R. O. Emerson, H. Robins, R. H. Pierce, D. A. Elashoff, C. Robert, A. Ribas, PD-1 blockade induces responses by inhibiting adaptive immune resistance. *Nature* **515**, 568-571 (2014).

14. J. Zhao, A. X. Chen, R. D. Gartrell, A. M. Silverman, L. Aparicio, T. Chu, D. Bordbar, D. Shan, J. Samanamud, A. Mahajan, I. Filip, R. Orenbuch, M. Goetz, J. T. Yamaguchi, M. Cloney, C. Horbinski, R. V. Lukas, J. Raizer, A. I. Rae, J. Yuan, P. Canoll, J. N. Bruce, Y. M. Saenger, P. Sims, F. M. Iwamoto, A. M. Sonabend, R. Rabadan, Immune and genomic correlates of response to anti-PD-1 immunotherapy in glioblastoma. *Nat Med* **25**, 462-469 (2019).

15. K. A. Schalper, M. E. Rodriguez-Ruiz, R. Diez-Valle, A. Lopez-Janeiro, A. Porciuncula, M. A. Idoate, S. Inoges, C. de Andrea, A. Lopez-Diaz de Cerio, S. Tejada, P. Berraondo, F. Villarroel-Espindola, J. Choi, A. Gurpide, M. Giraldez, I. Goicoechea, J. Gallego Perez-Larraya, M. F. Sanmamed, J. L. Perez-Gracia, I. Melero, Neoadjuvant nivolumab modifies the tumor immune microenvironment in resectable glioblastoma. *Nat Med* **25**, 470-476 (2019).

16. T. F. Cloughesy, A. Y. Mochizuki, J. R. Orpilla, W. Hugo, A. H. Lee, T. B. Davidson, A. C. Wang, B. M. Ellingson, J. A. Rytlewski, C. M. Sanders, E. S. Kawaguchi, L. Du, G. Li, W. H. Yong, S. C. Gaffey, A. L. Cohen, I. K. Mellinghoff, E. Q. Lee, D. A. Reardon, B. J. O'Brien, N. A. Butowski, P. L. Nghiemphu, J. L. Clarke, I. C. Arrillaga-Romany, H. Colman, T. J. Kaley, J. F. de Groot, L. M. Liau, P. Y. Wen, R. M. Prins, Neoadjuvant anti-PD-1 immunotherapy promotes a survival benefit with intratumoral and systemic immune responses in recurrent glioblastoma. *Nat Med* **25**, 477-486 (2019).

17. J. M. Taube, R. A. Anders, G. D. Young, H. Xu, R. Sharma, T. L. McMiller, S. Chen, A. P. Klein, D. M. Pardoll, S. L. Topalian, L. Chen, Colocalization of inflammatory response with B7-H1 expression in human melanocytic lesions supports an adaptive resistance mechanism of immune escape. *Sci Transl Med* **4**, 127ra137 (2012).

18. M. Ayers, J. Lunceford, M. Nebozhyn, E. Murphy, A. Loboda, D. R. Kaufman, A. Albright, J. D. Cheng, S. P. Kang, V. Shankaran, S. A. Piha-Paul, J. Yearley, T. Y. Seiwert, A. Ribas, T. K. McClanahan, IFN-gamma-related mRNA profile predicts clinical response to PD-1 blockade. *J Clin Invest* **127**, 2930-2940 (2017).

19. P. A. Ott, Y. J. Bang, S. A. Piha-Paul, A. R. A. Razak, J. Bennouna, J. C. Soria, H. S. Rugo, R. B. Cohen, B. H. O'Neil, J. M. Mehnert, J. Lopez, T. Doi, E. M. J. van Brummelen, R. Cristescu, P. Yang, K. Emancipator, K. Stein, M. Ayers, A. K. Joe, J. K. Lunceford, T-cell-inflamed gene-expression profile, programmed death ligand 1 expression, and tumor mutational burden predict efficacy in patients treated with pembrolizumab across 20 cancers: KEYNOTE-028. *J Clin Oncol* **37**, 318-327 (2019).

20. J. L. Benci, B. Xu, Y. Qiu, T. J. Wu, H. Dada, C. Twyman-Saint Victor, L. Cucolo, D. S. M. Lee, K. E. Pauken, A. C. Huang, T. C. Gangadhar, R. K. Amaravadi, L. M. Schuchter, M. D. Feldman, H. Ishwaran, R. H. Vonderheide, A. Maity, E. J. Wherry, A. J. Minn, Tumor interferon signaling regulates a multigenic resistance program to immune checkpoint blockade. *Cell* **167**, 1540-1554 e1512 (2016).

21. S. W. Ng, A. Mitchell, J. A. Kennedy, W. C. Chen, J. McLeod, N. Ibrahimova, A. Arruda, A. Popescu, V. Gupta, A. D. Schimmer, A. C. Schuh, K. W. Yee, L. Bullinger, T. Herold, D. Gorlich, T. Buchner, W. Hiddemann, W. E. Berdel, B. Wormann, M. Cheok, C. Preudhomme, H. Dombret, K. Metzeler, C. Buske, B. Lowenberg, P. J. Valk, P. W. Zandstra, M. D. Minden, J. E. Dick, J. C. Wang, A 17-gene stemness score for rapid determination of risk in acute leukaemia. *Nature* **540**, 433-437 (2016).

22. P. Danaher, S. Warren, A. Cesano, Development of gene expression signatures characterizing the tumor-immune interaction. *J Clin Oncol* **36**, 205-205 (2018).

23. P. Danaher, S. Warren, L. Dennis, L. D'Amico, A. White, M. L. Disis, M. A. Geller, K. Odunsi, J. Beechem, S. P. Fling, Gene expression markers of Tumor Infiltrating Leukocytes. *J Immunother Cancer* **5**, 18 (2017).

24. K. Mrozek, G. Marcucci, D. Nicolet, K. S. Maharry, H. Becker, S. P. Whitman, K. H. Metzeler, S. Schwind, Y. Z. Wu, J. Kohlschmidt, M. J. Pettenati, N. A. Heerema, A. W. Block, S. R. Patil, M. R. Baer, J. E. Kolitz, J. O. Moore, A. J. Carroll, R. M. Stone, R. A. Larson, C. D. Bloomfield, Prognostic significance of the European LeukemiaNet standardized system for reporting cytogenetic and molecular alterations in adults with acute myeloid leukemia. *J Clin Oncol* **30**, 4515-4523 (2012).

25. J. Vadakekolathu, T. Patel, S. Reeder, H. Schaarschmidt, M. Schmitz, M. Bornhäuser, S. E. Warren, T. Hood, P. Danaher, A. Cesano, J. M. Beechem, A. G. Pockley, S. K. Tasian, S. Rutella, Immune gene expression profiling in children and adults with acute myeloid leukemia identifies distinct phenotypic patterns. *Blood* **130**, 3942-3942 (2017).

26. S. Spranger, R. M. Spaapen, Y. Zha, J. Williams, Y. Meng, T. T. Ha, T. F. Gajewski, Up-regulation of PD-L1, IDO, and Tregs in the melanoma tumor microenvironment is driven by CD8+ T cells. *Sci Transl Med* **5**, 200ra116 (2013).

27. C. U. Blank, E. A. Rozeman, L. F. Fanchi, K. Sikorska, B. van de Wiel, P. Kvistborg, O. Krijgsman, M. van den Braber, D. Philips, A. Broeks, J. V. van Thienen, H. A. Mallo, S. Adriaansz, S. Ter Meulen, L. M. Pronk, L. G. Grijpink-Ongering, A. Bruining, R. M. Gittelman, S. Warren, H. van Tinteren, D. S. Peeper, J. Haanen, A. C. J. van Akkooi, T. N. Schumacher, Neoadjuvant versus adjuvant ipilimumab plus nivolumab in macroscopic stage III melanoma. *Nat Med* **24**, 1655-1661 (2018).

28. R. M. Zemek, E. De Jong, W. L. Chin, I. S. Schuster, V. S. Fear, T. H. Casey, C. Forbes, S. J. Dart, C. Leslie, A. Zaitouny, M. Small, L. Boon, A. R. R. Forrest, D. O. Muiri, M. A. Degli-Esposti, M. J. Millward, A. K. Nowak, T. Lassmann, A. Bosco, R. A. Lake, W. J. Lesterhuis, Sensitization to immune checkpoint blockade through activation of a STAT1/NK axis in the tumor microenvironment. *Sci Transl Med* **11**, (2019).

29. A. Ehninger, M. Kramer, C. Rollig, C. Thiede, M. Bornhauser, M. von Bonin, M. Wermke, A. Feldmann, M. Bachmann, G. Ehninger, U. Oelschlagel, Distribution and levels of cell surface expression of CD33 and CD123 in acute myeloid leukemia. *Blood Cancer J* **4**, e218 (2014).

30. G. Ciriello, E. Cerami, C. Sander, N. Schultz, Mutual exclusivity analysis identifies oncogenic network modules. *Genome Res* **22**, 398-406 (2012).

31. J. Versluis, F. E. In 't Hout, R. Devillier, W. L. van Putten, M. G. Manz, M. C. Vekemans, M. C. Legdeur, J. R. Passweg, J. Maertens, J. Kuball, B. J. Biemond, P. J. Valk, B. A. van der Reijden, G. Meloni, H. C. Schouten, E. Vellenga, T. Pabst, R. Willemze, B. Lowenberg, G. Ossenkoppele, F. Baron, G. Huls, J. J. Cornelissen, Comparative value of post-remission treatment in cytogenetically normal AML subclassified by NPM1 and FLT3-ITD allelic ratio. *Leukemia* **31**, 26-33 (2017).

32. S. Iacobelli, E. S. Committee, Suggestions on the use of statistical methodologies in studies of the European Group for Blood and Marrow Transplantation. *Bone Marrow Transplant* **48 Suppl 1**, S1-37 (2013).

33. B. C. Medeiros, Interpretation of clinical endpoints in trials of acute myeloid leukemia. *Leuk Res* **68**, 32-39 (2018).

34. J. E. Farrar, H. L. Schuback, R. E. Ries, D. Wai, O. A. Hampton, L. R. Trevino, T. A. Alonzo, J. M. Guidry Auvil, T. M. Davidsen, P. Gesuwan, L. Hermida, D. M. Muzny, N. Dewal, N. Rustagi, L. R. Lewis, A. S. Gamis, D. A. Wheeler, M. A. Smith, D. S. Gerhard, S. Meshinchi, Genomic profiling of pediatric acute myeloid leukemia reveals a changing mutational landscape from disease diagnosis to relapse. *Cancer Res* **76**, 2197-2205 (2016).

35. H. Bolouri, J. E. Farrar, T. Triche, Jr., R. E. Ries, E. L. Lim, T. A. Alonzo, Y. Ma, R. Moore, A. J. Mungall, M. A. Marra, J. Zhang, X. Ma, Y. Liu, Y. Liu, J. M. G. Auvil, T. M. Davidsen, P. Gesuwan, L. C. Hermida, B. Salhia, S. Capone, G. Ramsingh, C. M.

Zwaan, S. Noort, S. R. Piccolo, E. A. Kolb, A. S. Gamis, M. A. Smith, D. S. Gerhard, S. Meshinchi, The molecular landscape of pediatric acute myeloid leukemia reveals recurrent structural alterations and age-specific mutational interactions. *Nat Med* **24**, 103-112 (2018).

36.   R. G. Majzner, S. Heitzeneder, C. L. Mackall, Harnessing the immunotherapy revolution for the treatment of childhood cancers. *Cancer Cell* **31**, 476-485 (2017).

37.   S. S. Chung, W. S. Eng, W. Hu, M. Khalaj, F. E. Garrett-Bakelman, M. Tavakkoli, R. L. Levine, M. Carroll, V. M. Klimek, A. M. Melnick, C. Y. Park, CD99 is a therapeutic target on disease stem cells in myeloid malignancies. *Sci Transl Med* **9**, (2017).

38.   H. A. Knaus, S. Berglund, H. Hackl, A. L. Blackford, J. F. Zeidner, R. Montiel-Esparza, R. Mukhopadhyay, K. Vanura, B. R. Blazar, J. E. Karp, L. Luznik, I. Gojo, Signatures of CD8+ T cell dysfunction in AML patients and their reversibility with response to chemotherapy. *JCI Insight* **3**, e120974 (2018).

39.   D. V. Dolfi, K. D. Mansfield, A. M. Polley, S. A. Doyle, G. J. Freeman, H. Pircher, K. E. Schmader, E. J. Wherry, Increased T-bet is associated with senescence of influenza virus-specific CD8 T cells in aged humans. *J Leukoc Biol* **93**, 825-836 (2013).

40.   M. A. Paley, D. C. Kroy, P. M. Odorizzi, J. B. Johnnidis, D. V. Dolfi, B. E. Barnett, E. K. Bikoff, E. J. Robertson, G. M. Lauer, S. L. Reiner, E. J. Wherry, Progenitor and terminal subsets of CD8+ T cells cooperate to contain chronic viral infection. *Science* **338**, 1220-1225 (2012).

41.   R. B. Walter, M. Othus, G. Borthakur, F. Ravandi, J. E. Cortes, S. A. Pierce, F. R. Appelbaum, H. A. Kantarjian, E. H. Estey, Prediction of early death after induction therapy for newly diagnosed acute myeloid leukemia with pretreatment risk scores: a novel paradigm for treatment assignment. *J Clin Oncol* **29**, 4417-4423 (2011).

42.   R. R. Weichselbaum, H. Ishwaran, T. Yoon, D. S. Nuyten, S. W. Baker, N. Khodarev, A. W. Su, A. Y. Shaikh, P. Roach, B. Kreike, B. Roizman, J. Bergh, Y. Pawitan, M. J. van de Vijver, A. J. Minn, An interferon-related gene signature for DNA damage resistance is a predictive marker for chemotherapy and radiation for breast cancer. *Proc Natl Acad Sci U S A* **105**, 18490-18495 (2008).

43.   J. W. Tyner, C. E. Tognon, D. Bottomly, B. Wilmot, S. E. Kurtz, S. L. Savage, N. Long, A. R. Schultz, E. Traer, M. Abel, A. Agarwal, A. Blucher, U. Borate, J. Bryant, R. Burke, A. Carlos, R. Carpenter, J. Carroll, B. H. Chang, C. Coblentz, A. d'Almeida, R. Cook, A. Danilov, K. T. Dao, M. Degnin, D. Devine, J. Dibb, D. K. t. Edwards, C. A. Eide, I. English, J. Glover, R. Henson, H. Ho, A. Jemal, K. Johnson, R. Johnson, B. Junio, A. Kaempf, J. Leonard, C. Lin, S. Q. Liu, P. Lo, M. M. Loriaux, S. Luty, T. Macey, J. MacManiman, J. Martinez, M. Mori, D. Nelson, C. Nichols, J. Peters, J. Ramsdill, A. Rofelty, R. Schuff, R. Searles, E. Segerdell, R. L. Smith, S. E. Spurgeon, T. Sweeney, A. Thapa, C. Visser, J. Wagner, K. Watanabe-Smith, K. Werth, J. Wolf, L. White, A. Yates, H. Zhang, C. R. Cogle, R. H. Collins, D. C. Connolly, M. W. Deininger, L. Drusbosky, C. S. Hourigan, C. T. Jordan, P. Kropf, T. L. Lin, M. E. Martinez, B. C. Medeiros, R. R. Pallapati, D. A. Pollyea, R. T. Swords, J. M. Watts, S. J. Weir, D. L. Wiest, R. M. Winters, S. K. McWeeney, B. J. Druker, Functional genomic landscape of acute myeloid leukaemia. *Nature* **562**, 526-531 (2018).

44.   P. J. Valk, R. G. Verhaak, M. A. Beijen, C. A. Erpelinck, S. Barjesteh van Waalwijk van Doorn-Khosrovani, J. M. Boer, H. B. Beverloo, M. J. Moorhouse, P. J. van der Spek, B. Lowenberg, R. Delwel, Prognostically useful gene-expression profiles in acute myeloid leukemia. *N Engl J Med* **350**, 1617-1628 (2004).

45.   S. Wagner, J. Vadakekolathu, S. K. Tasian, H. Altmann, M. Bornhauser, A. G. Pockley, G. R. Ball, S. Rutella, A parsimonious 3-gene signature predicts clinical outcomes in an acute myeloid leukemia multicohort study. *Blood Adv* **3**, 1330-1346 (2019).

46.   M. Bezzi, N. Seitzer, T. Ishikawa, M. Reschke, M. Chen, G. Wang, C. Mitchell, C. Ng, J. Katon, A. Lunardi, S. Signoretti, J. G. Clohessy, J. Zhang, P. P. Pandolfi, Diverse

genetic-driven immune landscapes dictate tumor progression through distinct mechanisms. *Nat Med* **24**, 165-175 (2018).

47.   E. K. Cook, T. Izukawa, S. Young, G. Rosen, M. Jamali, L. Zhang, D. Johnson, E. Bain, J. Hilland, C. K. Ferrone, J. Buckstein, J. Francis, B. Momtaz, A. J. M. McNaughton, X. Liu, B. Snetsinger, R. Buckstein, M. J. Rauh, Comorbid and inflammatory characteristics of genetic subtypes of clonal hematopoiesis. *Blood Adv* **3**, 2482-2486 (2019).

48.   G. R. Chichili, L. Huang, H. Li, S. Burke, L. He, Q. Tang, L. Jin, S. Gorlatov, V. Ciccarone, F. Chen, S. Koenig, M. Shannon, R. Alderson, P. A. Moore, S. Johnson, E. Bonvini, A CD3xCD123 bispecific DART for redirecting host T cells to myelogenous leukemia: preclinical activity and safety in nonhuman primates. *Sci Transl Med* **7**, 289ra282 (2015).

49.   R. B. Walter, M. Othus, A. K. Burnett, B. Lowenberg, H. M. Kantarjian, G. J. Ossenkoppele, R. K. Hills, F. Ravandi, T. Pabst, A. Evans, S. R. Pierce, M. C. Vekemans, F. R. Appelbaum, E. H. Estey, Resistance prediction in AML: analysis of 4601 patients from MRC/NCRI, HOVON/SAKK, SWOG and MD Anderson Cancer Center. *Leukemia* **29**, 312-320 (2015).

50.   T. Herold, V. Jurinovic, A. M. N. Batcha, S. A. Bamopoulos, M. Rothenberg-Thurley, B. Ksienzyk, L. Hartmann, P. A. Greif, J. Phillippou-Massier, S. Krebs, H. Blum, S. Amler, S. Schneider, N. Konstandin, M. C. Sauerland, D. Gorlich, W. E. Berdel, B. J. Wormann, J. Tischer, M. Subklewe, S. K. Bohlander, J. Braess, W. Hiddemann, K. H. Metzeler, U. Mansmann, K. Spiekermann, A 29-gene and cytogenetic score for the prediction of resistance to induction treatment in acute myeloid leukemia. *Haematologica* **103**, 456-465 (2018).

51.   R. Radpour, C. Riether, C. Simillion, S. Hopner, R. Bruggmann, A. F. Ochsenbein, CD8+ T cells expand stem and progenitor cells in favorable but not adverse risk acute myeloid leukemia. *Leukemia* **33**, 2379-2392 (2019).

52.   N. N. Khodarev, M. Beckett, E. Labay, T. Darga, B. Roizman, R. R. Weichselbaum, STAT1 is overexpressed in tumors selected for radioresistance and confers protection from radiation in transduced sensitive cells. *Proc Natl Acad Sci U S A* **101**, 1714-1719 (2004).

53.   Q. Han, N. Bagheri, E. M. Bradshaw, D. A. Hafler, D. A. Lauffenburger, J. C. Love, Polyfunctional responses by human T cells result from sequential release of cytokines. *Proc Natl Acad Sci U S A* **109**, 1607-1612 (2012).

54.   M. J. Christopher, A. A. Petti, M. P. Rettig, C. A. Miller, E. Chendamarai, E. J. Duncavage, J. M. Klco, N. M. Helton, M. O'Laughlin, C. C. Fronick, R. S. Fulton, R. K. Wilson, L. D. Wartman, J. S. Welch, S. E. Heath, J. D. Baty, J. E. Payton, T. A. Graubert, D. C. Link, M. J. Walter, P. Westervelt, T. J. Ley, J. F. DiPersio, Immune Escape of Relapsed AML Cells after Allogeneic Transplantation. *N Engl J Med* **379**, 2330-2341 (2018).

55.   J. Li, K. T. Byrne, F. Yan, T. Yamazoe, Z. Chen, T. Baslan, L. P. Richman, J. H. Lin, Y. H. Sun, A. J. Rech, D. Balli, C. A. Hay, Y. Sela, A. J. Merrell, S. M. Liudahl, N. Gordon, R. J. Norgard, S. Yuan, S. Yu, T. Chao, S. Ye, T. S. K. Eisinger-Mathason, R. B. Faryabi, J. W. Tobias, S. W. Lowe, L. M. Coussens, E. J. Wherry, R. H. Vonderheide, B. Z. Stanger, Tumor cell-intrinsic factors underlie heterogeneity of immune cell infiltration and response to immunotherapy. *Immunity* **49**, 178-193 e177 (2018).

56.   J. J. Luke, R. Bao, R. F. Sweis, S. Spranger, T. F. Gajewski, WNT/beta-catenin pathway activation correlates with immune exclusion across human cancers. *Clin Cancer Res*, (2019).

57.   Y. Senbabaoglu, R. S. Gejman, A. G. Winer, M. Liu, E. M. Van Allen, G. de Velasco, D. Miao, I. Ostrovnaya, E. Drill, A. Luna, N. Weinhold, W. Lee, B. J. Manley, D. N. Khalil, S. D. Kaffenberger, Y. Chen, L. Danilova, M. H. Voss, J. A. Coleman, P. Russo, V. E. Reuter, T. A. Chan, E. H. Cheng, D. A. Scheinberg, M. O. Li, T. K. Choueiri, J. J. Hsieh, C. Sander, A. A. Hakimi, Tumor immune microenvironment

characterization in clear cell renal cell carcinoma identifies prognostic and immunotherapeutically relevant messenger RNA signatures. *Genome Biol* **17**, 231 (2016).

58. Z. Y. Dong, W. Z. Zhong, X. C. Zhang, J. Su, Z. Xie, S. Y. Liu, H. Y. Tu, H. J. Chen, Y. L. Sun, Q. Zhou, J. J. Yang, X. N. Yang, J. X. Lin, H. H. Yan, H. R. Zhai, L. X. Yan, R. Q. Liao, S. P. Wu, Y. L. Wu, Potential predictive value of TP53 and KRAS mutation status for response to PD-1 blockade immunotherapy in lung adenocarcinoma. *Clin Cancer Res* **23**, 3012-3024 (2017).

59. J. S. Welch, A. A. Petti, C. A. Miller, C. C. Fronick, M. O'Laughlin, R. S. Fulton, R. K. Wilson, J. D. Baty, E. J. Duncavage, B. Tandon, Y. S. Lee, L. D. Wartman, G. L. Uy, A. Ghobadi, M. H. Tomasson, I. Pusic, R. Romee, T. A. Fehniger, K. E. Stockerl-Goldstein, R. Vij, S. T. Oh, C. N. Abboud, A. F. Cashen, M. A. Schroeder, M. A. Jacoby, S. E. Heath, K. Luber, M. R. Janke, A. Hantel, N. Khan, M. J. Sukhanova, R. W. Knoebel, W. Stock, T. A. Graubert, M. J. Walter, P. Westervelt, D. C. Link, J. F. DiPersio, T. J. Ley, TP53 and decitabine in acute myeloid leukemia and myelodysplastic syndromes. *N Engl J Med* **375**, 2023-2036 (2016).

60. W. Peng, J. Q. Chen, C. Liu, S. Malu, C. Creasy, M. T. Tetzlaff, C. Xu, J. A. McKenzie, C. Zhang, X. Liang, L. J. Williams, W. Deng, G. Chen, R. Mbofung, A. J. Lazar, C. A. Torres-Cabala, Z. A. Cooper, P. L. Chen, T. N. Tieu, S. Spranger, X. Yu, C. Bernatchez, M. A. Forget, C. Haymaker, R. Amaria, J. L. McQuade, I. C. Glitza, T. Cascone, H. S. Li, L. N. Kwong, T. P. Heffernan, J. Hu, R. L. Bassett, Jr., M. W. Bosenberg, S. E. Woodman, W. W. Overwijk, G. Lizee, J. Roszik, T. F. Gajewski, J. A. Wargo, J. E. Gershenwald, L. Radvanyi, M. A. Davies, P. Hwu, Loss of PTEN promotes resistance to T cell-mediated immunotherapy. *Cancer Discov* **6**, 202-216 (2016).

61. S. George, D. Miao, G. D. Demetri, D. Adeegbe, S. J. Rodig, S. Shukla, M. Lipschitz, A. Amin-Mansour, C. P. Raut, S. L. Carter, P. Hammerman, G. J. Freeman, C. J. Wu, P. A. Ott, K. K. Wong, E. M. Van Allen, Loss of PTEN Is associated with resistance to anti-PD-1 checkpoint blockade therapy in metastatic uterine leiomyosarcoma. *Immunity* **46**, 197-204 (2017).

62. B. P. Fairfax, C. A. Taylor, R. A. Watson, I. Nassiri, S. Danielli, H. Fang, E. A. Mahe, R. Cooper, V. Woodcock, Z. Traill, M. H. Al-Mossawi, J. C. Knight, P. Klenerman, M. Payne, M. R. Middleton, Peripheral CD8(+) T cell characteristics associated with durable responses to immune checkpoint blockade in patients with metastatic melanoma. *Nat Med* **26**, 193-199 (2020).

63. T. D. Wu, S. Madireddi, P. E. de Almeida, R. Banchereau, Y. J. Chen, A. S. Chitre, E. Y. Chiang, H. Iftikhar, W. E. O'Gorman, A. Au-Yeung, C. Takahashi, L. D. Goldstein, C. Poon, S. Keerthivasan, D. E. de Almeida Nagata, X. Du, H. M. Lee, K. L. Banta, S. Mariathasan, M. Das Thakur, M. A. Huseni, M. Ballinger, I. Estay, P. Caplazi, Z. Modrusan, L. Delamarre, I. Mellman, R. Bourgon, J. L. Grogan, Peripheral T cell expansion predicts tumour infiltration and clinical response. *Nature*, (2020).

64. T. Sugio, K. Miyawaki, K. Kato, K. Sasaki, K. Yamada, J. Iqbal, T. Miyamoto, K. Ohshima, T. Maeda, H. Miyoshi, K. Akashi, Microenvironmental immune cell signatures dictate clinical outcomes for PTCL-NOS. *Blood Adv* **2**, 2242-2252 (2018).

65. J. E. Payton, N. R. Grieselhuber, L. W. Chang, M. Murakami, G. K. Geiss, D. C. Link, R. Nagarajan, M. A. Watson, T. J. Ley, High throughput digital quantification of mRNA abundance in primary human acute myeloid leukemia samples. *J Clin Invest* **119**, 1714-1726 (2009).

66. A. Subramanian, P. Tamayo, V. K. Mootha, S. Mukherjee, B. L. Ebert, M. A. Gillette, A. Paulovich, S. L. Pomeroy, T. R. Golub, E. S. Lander, J. P. Mesirov, Gene set enrichment analysis: a knowledge-based approach for interpreting genome-wide expression profiles. *Proc Natl Acad Sci U S A* **102**, 15545-15550 (2005).

67. S. Rutella, J. Vadakekolathu, H. Altmann, T. Patel, S. Reeder, Y. Liang, M. Schmitz, T. Hood, P. Danaher, S. Warren, A. Cesano, J. M. Beechem, A. G. Pockley, S. K.

Tasian, M. Bornhäuser, Capturing the complexity of the immune microenvironment of acute myeloid leukemia with 3D biology technology. *J Clin Oncol* **36**, 50-50 (2018).

68. V. Stavropoulou, S. Kaspar, L. Brault, M. A. Sanders, S. Juge, S. Morettini, A. Tzankov, M. Iacovino, I. J. Lau, T. A. Milne, H. Royo, M. Kyba, P. J. M. Valk, A. Peters, J. Schwaller, MLL-AF9 expression in hematopoietic stem cells drives a highly invasive AML expressing EMT-related genes linked to poor outcome. *Cancer Cell* **30**, 43-58 (2016).

69. T. J. Ley, C. Miller, L. Ding, B. J. Raphael, A. J. Mungall, A. Robertson, K. Hoadley, T. J. Triche, Jr., P. W. Laird, J. D. Baty, L. L. Fulton, R. Fulton, S. E. Heath, J. Kalicki-Veizer, C. Kandoth, J. M. Klco, D. C. Koboldt, K. L. Kanchi, S. Kulkarni, T. L. Lamprecht, D. E. Larson, L. Lin, C. Lu, M. D. McLellan, J. F. McMichael, J. Payton, H. Schmidt, D. H. Spencer, M. H. Tomasson, J. W. Wallis, L. D. Wartman, M. A. Watson, J. Welch, M. C. Wendl, A. Ally, M. Balasundaram, I. Birol, Y. Butterfield, R. Chiu, A. Chu, E. Chuah, H. J. Chun, R. Corbett, N. Dhalla, R. Guin, A. He, C. Hirst, M. Hirst, R. A. Holt, S. Jones, A. Karsan, D. Lee, H. I. Li, M. A. Marra, M. Mayo, R. A. Moore, K. Mungall, J. Parker, E. Pleasance, P. Plettner, J. Schein, D. Stoll, L. Swanson, A. Tam, N. Thiessen, R. Varhol, N. Wye, Y. Zhao, S. Gabriel, G. Getz, C. Sougnez, L. Zou, M. D. Leiserson, F. Vandin, H. T. Wu, F. Applebaum, S. B. Baylin, R. Akbani, B. M. Broom, K. Chen, T. C. Motter, K. Nguyen, J. N. Weinstein, N. Zhang, M. L. Ferguson, C. Adams, A. Black, J. Bowen, J. Gastier-Foster, T. Grossman, T. Lichtenberg, L. Wise, T. Davidsen, J. A. Demchok, K. R. Shaw, M. Sheth, H. J. Sofia, L. Yang, J. R. Downing, G. Eley, Genomic and epigenomic landscapes of adult de novo acute myeloid leukemia. *N Engl J Med* **368**, 2059-2074 (2013).

70. R. Edgar, M. Domrachev, A. E. Lash, Gene Expression Omnibus: NCBI gene expression and hybridization array data repository. *Nucleic Acids Res* **30**, 207-210 (2002).

71. T. Metsalu, J. Vilo, ClustVis: a web tool for visualizing clustering of multivariate data using Principal Component Analysis and heatmap. *Nucleic Acids Res* **43**, W566-570 (2015).

72. Z. Tang, B. Kang, C. Li, T. Chen, Z. Zhang, GEPIA2: an enhanced web server for large-scale expression profiling and interactive analysis. *Nucleic Acids Res* **47**, W556-W560 (2019).

73. M. Lauten, A. Moricke, R. Beier, M. Zimmermann, M. Stanulla, B. Meissner, E. Odenwald, A. Attarbaschi, C. Niemeyer, F. Niggli, H. Riehm, M. Schrappe, Prediction of outcome by early bone marrow response in childhood acute lymphoblastic leukemia treated in the ALL-BFM 95 trial: differential effects in precursor B-cell and T-cell leukemia. *Haematologica* **97**, 1048-1056 (2012).

74. W. Kern, T. Haferlach, C. Schoch, H. Loffler, W. Gassmann, A. Heinecke, M. C. Sauerland, W. Berdel, T. Buchner, W. Hiddemann, Early blast clearance by remission induction therapy is a major independent prognostic factor for both achievement of complete remission and long-term outcome in acute myeloid leukemia: data from the German AML Cooperative Group (AMLCG) 1992 Trial. *Blood* **101**, 64-70 (2003).

Acknowledgments

Author contributions

Concept and design: S. Rutella

Development of methodology: J. Vadakekolathu, T. Hood, S.E. Church, S. Reeder, S.E. Warren, Y. Liang, T.H. Smith, M.D. Bailey, J. Gowen-MacDonald, S. Rutella

Acquired, consented and managed patients; processed patient samples: M.D. Minden, H. Altmann, T. Patel, N. Ibrahimova, A. Arruda, J. Muth, P.J.M. Valk, B. Löwenberg, M. Bornhäuser, S.K. Tasian, M.P. Rettig, J.F. DiPersio

Analysis and interpretation of data: J. Vadakekolathu, M.D. Minden, T. Hood, S.E. Church, S. Reeder, A.H. Sullivan, E.J. Viboch, S.E. Warren, Y. Liang, T.H. Smith, G.A. Foulds, M.D. Bailey, J. Gowen-MacDonald, M. Schmitz, A. Cesano, P.J.M. Valk, B. Löwenberg, A.G. Pockley, M. Bornhäuser, S.K. Tasian, J. Davidson-Moncada, J.F. DiPersio, S. Rutella

Clinical trial implementation: J.F. DiPersio was principal investigator at Washington University in St. Louis, St. Louis, United States of America. B. Löwenberg was principal investigator at Erasmus University Medical Centre, Rotterdam, Netherlands.

Writing of the manuscript: S. Rutella

Review and/or revision of the manuscript: J. Vadakekolathu, M.D. Minden, T. Hood, S.E. Church, E.J. Viboch, S.E. Warren, G.A. Foulds, M. Schmitz, A. Cesano, P.J.M. Valk, B. Löwenberg, A.G. Pockley, M. Bornhäuser, S.K. Tasian, M.P. Rettig, J. Davidson-Moncada, J.F. DiPersio, S. Rutella

Study supervision: S. Rutella

Figure Legends

Fig. 1: Immune gene sets stratify bone marrow samples from patients with newly diagnosed AML. **A**) Unsupervised hierarchical clustering (Euclidean distance, complete linkage) of the correlation matrix of immune and biological activity signatures identifies co-expression patterns (grey boxes) of immune gene sets (correlation value color-coded *per* the legend, where blue denotes a Pearson correlation coefficient of -1.0 and red indicates a Pearson correlation coefficient of 1.0) in the bone marrow (BM) microenvironment of patients with AML (PMCC cohort; n=290), namely, IFN-dominant, adaptive and myeloid gene modules. Immune cell type (*23*) and signature scores (*22*) were calculated from mRNA expression as pre-defined linear combinations (weighted averages) of biologically relevant gene sets. Morpheus, an online tool developed at the Broad Institute (MA, USA) was used for data analysis and visualization. **B**) IFN-dominant, adaptive and myeloid scores in aggregate stratify patients with newly diagnosed AML into two distinct clusters, which are referred in this study as immune-infiltrated and immune-depleted (*25*). ClustVis, an online tool for clustering of multivariate data, was used for data analysis and visualization (*71*). **C**) Violin plots summarizing the expression of IFN-stimulated genes (ISGs), T-cell and cytotoxicity markers, negative immune checkpoints, genes implicated in antigen processing and presentation, and immunotherapy targets in AML cases with an immune-infiltrated and immune-depleted tumor microenvironment (TME). Data were compared using the Mann-Whitney *U* test for unpaired data (two-sided). *$P < 0.05$; ***$P < 0.0001$. **D**) Spearman correlation coefficients between *STAT1*, ISGs [*IRF1*, *MX1*, *IFIT1*, *TNFRSF14, PD-L1* (CD274)], surrogate markers for cytotoxic T cells (*CD8A*, *GZMA*) and negative immune checkpoints [*LAG3*, *HAVCR2* (Tim-3)] under conditions of high and low immune infiltration.

Fig. 2: Multiplexed protein detection with GeoMx DSP identifies prognostic signatures in immune-infiltrated AML. A) CD3 hotspots (green fluorescence) in representative regions of interest (ROIs) from a bone marrow (BM) trephine biopsy obtained at time of AML diagnosis (SAL series). **B**) Association between PTEN and CD8/GZMB expression in geometric ROIs

(n=240) from 10 BM FFPE sections (median split of PTEN barcode counts). Comparisons of CD8 and GZMB expression between PTEN^{high} and PTEN^{low} ROIs were performed using the Mann-Whitney U test for unpaired data (two-sided). **C**) Correlation matrix of protein expression in BM biopsies from 10 patients with newly diagnosed AML (SAL series). Protein expression data was subjected to unsupervised hierarchical clustering. Heatmaps were built using Morpheus with blue boxes denoting four distinct protein co-expression patterns (Pearson correlation coefficient >0.45) or signatures (SIG). **D**) Abnormalities in SIG3 genes (mRNA upregulation, gene amplification, deep deletion and mis-sense mutations, relative to the gene's expression distribution in all profiled AML samples) in TCGA cases. Data were retrieved, analyzed and visualized using cBioPortal. Abnormalities in only one gene utilized in the query (by default, non-synonymous mutations, fusions, amplifications and deep deletions) were sufficient to define that particular patient sample as "altered". **E**) GO enrichment analysis. For the gene list submitted to metascape.org, pathway and process enrichment analyses were carried out using all genes in the genome as the enrichment background. Terms with a P value < 0.01, a minimum count of 3, and an enrichment factor >1.5 (defined as the ratio between the observed counts and the counts expected by chance) were collected and grouped into clusters based on their membership similarities. **F**) Heatmap of immune cell type-specific scores and biological activity scores in TCGA-AML cases with and without abnormalities (Alt.) of SIG3 genes. ClustVis was used for data analysis and visualization (*71*). **G**) Kaplan-Meier estimates of relapse-free survival (RFS) and overall survival (OS) in TCGA-AML patients with (red line) and without (blue line) abnormalities of SIG3 genes. HR = hazard ratio. Survival curves were compared using a log-rank (Mantel-Cox) test.

Fig. 3: Clinical correlates of immune profiles in patients with newly diagnosed AML. **A**) Stratification of patient survival (PMCC cohort; n=290) within each ELN cytogenetic risk category by immune subtype (immune-infiltrated and immune-depleted). Kaplan-Meier estimates of RFS and OS are shown. Survival curves were compared using a log-rank (Mantel-Cox) test. *P < 0.05; **P < 0.01. HR=hazard ratio; CI=confidence interval. **B**)

Expression of PD1 and markers of CD8$^+$ T-cell exhaustion across cytogenetically defined patient categories. Data were compared using the Kruskal-Wallis test for unpaired determinations. FAV=favorable ELN risk; INT=intermediate ELN risk; ADV=adverse ELN risk. **C**) Cytogenetically defined categories stratify survival in patients with immune-infiltrated AML. Kaplan-Meier estimates of RFS and OS are shown. Survival curves were compared using a log-rank (Mantel-Cox) test. ***P < 0.001. **D**) Molecularly defined categories stratify survival in ELN intermediate AML cases (n=100) with immune-infiltrated and immune-depleted mRNA profiles. Patients were subclassified into molecular low risk (*NPM1* mutations without *FLT3*-ITD), molecular intermediate risk (*NPM1* wild-type without *FLT3*-ITD or with low *FLT3*-ITD allelic ratio) and molecular high risk (*NPM1* wild-type with *FLT3*-ITD), as previously reported (*31*). Kaplan-Meier estimates of OS are shown. Survival curves were compared using a log-rank (Mantel-Cox) test. ***P < 0.001. **E**) AUROC curve measuring the predictive ability of molecular risk (blue curve) and immune subtype (red curve) for OS. SE=standard error; CI=confidence interval. AUROC=1.0 would denote perfect prediction and AUROC=0.5 would denote no predictive ability.

Fig. 4: A 21-gene classifier stratifies survival in ELN-intermediate risk AML (n=100). **A**) Expression of the 21 differentially expressed (DE) genes across the PMCC discovery cohort (unsupervised hierarchical clustering; Euclidean distance; complete linkage). FDR=false discovery rate. Morpheus was used for data analysis and visualization. **B**) Expression of the 21 DE genes in patients with immune-infiltrated and immune-depleted AML. Data were compared using the Mann-Whitney U test for unpaired determinations. Red bars indicate median values. **C**) DE genes between favorable and adverse-risk AML were mapped to gene ontology (GO) biological processes and pathways using Metascape.org. **D**) Kaplan-Meier estimate of RFS and OS in patients with ELN intermediate-risk AML stratified by the 21-gene classifier. Survival curves were compared using a log-rank (Mantel-Cox) test. HR=hazard ratio; CI=confidence interval. **P < 0.01; ***P < 0.001. **E**) Kaplan-Meier estimate of OS in TCGA AML cases (first independent validation cohort) stratified by the 21-gene classifier

(median split of gene expression values). Data were accessed, analyzed and visualized through the Gene Expression Profiling Interactive Analysis (GEPIA) portal (http://gepia2.cancer-pku.cn/#survival) (*72*). Survival curves were compared using a log-rank (Mantel-Cox) test. **F**) Kaplan-Meier estimate of OS in HOVON AML cases (second independent validation cohort) stratified by the 21-gene classifier (median split of gene expression values). Survival curves were compared using a log-rank (Mantel-Cox) test. ****P < 0.0001.

Fig. 5: **Differentially expressed immune genes across age groups and disease stages**. **A**) Top 20 differentially expressed (DE) immune genes between childhood (n=34) and adult AML cases (n=46). ClustVis was used for data analysis and visualization. Violin plots summarize the expression of relevant chemokine genes. Data were compared using the Mann-Whitney *U* test for paired determinations. Volcano plots of DE genes were generated using the nSolver software package. ****P < 0.0001. **B**) Top 20 DE immune genes between matched BM samples from 22 adult patients (SAL cohort) at diagnosis and achievement of complete remission (CR). Data were compared using the Mann-Whitney *U* test for paired determinations. Volcano plots of DE genes were generated using the nSolver software package. ***P < 0.001; ****P < 0.0001. Data were compared using the Mann-Whitney *U* test for paired determinations. **C**) Top 20 DE immune genes between matched BM samples from 22 adult patients (SAL cohort) at diagnosis and disease relapse. Data were compared using the Mann-Whitney *U* test for paired determinations. Volcano plots of DE genes were generated using the nSolver software package. **P < 0.01; ***P < 0.001. **D**) Venn diagram showing overlap in DE genes between children and adults with AML, and patients at disease onset, achievement of CR and relapse.

Fig. 6: IFN-related mRNA profiles predict therapeutic resistance. **A**) Binary logistic regression predicting therapeutic response from IFN-related scores and conventional prognosticators, i.e., ELN cytogenetic risk category, WBC count at diagnosis, disease type

(primary *versus* secondary AML), and patient age at diagnosis (PMCC discovery cohort). AUROC=area under receiver operating characteristic. The dotted line indicates currently accepted thresholds (>0.80) of AUROC with good predictive ability in AML (*49*). **B**) AUROC curves measuring the predictive ability of ELN cytogenetic risk and IFN-related scores for therapeutic response (PMCC discovery cohort; n=290). SE=standard error; CI=confidence interval. AUROC=1.0 would denote perfect prediction and AUROC=0.5 would denote no predictive ability. **C**) AUROC curves measuring the predictive ability of ELN cytogenetic risk and IFN-related scores for therapeutic response in Beat AML trial specimens (validation cohort). SE=standard error; CI=confidence interval. **D**) Unsupervised hierarchical clustering (Euclidean distance, complete linkage) of the correlation matrix of immune and biological activity signatures identifies co-expression patterns of immune gene sets (correlation value color-coded *per* the legend; Pearson correlation coefficient >0.45; blue boxes) in the bone marrow (BM) microenvironment of AML patients in the HOVON series (n=618 cases with therapy response and ELN cytogenetic risk information). **E**) IFN-dominant, adaptive and myeloid scores in patients in the HOVON series. The Venn diagram shows the overlap between curated hallmark gene sets linked to IFN-γ responses (n=186) and inflammatory responses (n=189). MSigDB=Molecular Signature Database. **F**) Gene set enrichment analysis (GSEA) plots representing the normalized enrichment score (NES) of hallmark IFN-γ-response genes, inflammatory response genes and a subset of overlapping genes (n=36) between IFN-γ and inflammatory gene sets in AML patients in the HOVON series who failed to respond to induction chemotherapy. Gene sets were downloaded from the MSigDB. Each run was performed with 1,000 permutations. FDR=false discovery rate.

Fig. 7: Immune subtypes associate with response to flotetuzumab immunotherapy. A) Unsupervised hierarchical clustering (Euclidean distance, complete linkage) of immune and biological activity signatures in the BM microenvironment of patients with relapsed/refractory AML (n=30) receiving flotetuzumab immunotherapy in the CP-MGD006-01 clinical trial

(NCT#02152956). Anti-leukemic response was defined as detailed in Materials and Methods. **B**) IFN-module and tumor inflammation signature (TIS) scores in baseline BM samples from patients with primary refractory and relapsed AML. Red dots denote patients with evidence of anti-leukemic activity of flotetuzumab. Horizontal lines indicate median values. Comparisons were performed using the Mann-Whitney *U* test for unpaired data (two-sided). **$P < 0.01$. **C**) Area under receiver operating characteristic (AUROC) curves measuring the predictive ability of the IFN-module score and TIS scores for therapeutic response to flotetuzumab. CI=confidence interval. **D**) Immune activation in the TME during flotetuzumab treatment (matched BM samples from 19 patients). Red dots denote patients with evidence of flotetuzumab anti-leukemic activity. Horizontal lines indicate median values. Comparisons were performed with the Mann-Whitney *U* test for paired data (two-sided). Pre=baseline. C1=cycle 1. **$P < 0.01$. ***$P < 0.001$. **E**) Principal component analysis (PCA) of GeoMx DSP housekeeping-normalized barcode counts for 52 proteins from 11 pre-treatment and 8 matched post-cycle 1 (C1) BM samples with 5-35 regions of interest (ROIs) profiling the entire FFPE biopsy (**Fig. S12**). Points are colored by no response (NR; pink) or complete response (CR; green). **F**) Identification of CD3 hotspots in ROIs from a BM biopsy of a representative patient who achieved CR after flotetuzumab immunotherapy. CD3$^+$ T cells are shown in yellow. **G**) Differential expression of immuno-oncology (IO)-related proteins between baseline and post-C1 FFPE BM biopsies from two patients achieving CR after flotetuzumab immunotherapy. Analysis was performed using a linear mixed effect model. Vertical dotted lines represent ± 0.5 log2 fold change (FC) and the horizontal dotted line indicates a *P* value of 0.05. NS=not significant. **H**) Differential expression of IO-related proteins between ROIs with or without CD3 hotspots in two patient samples after 1 cycle of flotetuzumab who achieved CR. Analysis was performed using a linear mixed effect model. Vertical dotted lines represent ± 0.5 log2 fold-change and the horizontal dotted line indicates a *P* value of 0.05.

Table 1. AML cohorts selected for targeted immune gene expression profiling

Patient series	PMCC	CHOP	SAL
# of patients	290	34	46
Age (0-39), *n*	76	34	13
Age (40-59), *n*	126	0	19
Age (≥ 60), *n*	88	0	14
Median age (years, range)	52 (18-81)	10 (0.1-20)	53.5 (23-75)
WBC count at presentation	19.15 × 10^3/µL (0.7-399)	N.A.	56. 45 × 10^3/µL (0.84-320.2)
Cytogenetic risk group, *n*			
ELN favorable	35	8	10
ELN intermediate	155	20	27
ELN adverse	59	6	4
N.A.	41	-	5
Disease status at time of BM sampling, *n*			
Diagnosis	290	34	46
Complete remission	0	16	21
Relapse	0	11	24
# of BM samples analyzed	290	61	91
# of BM samples analyzed using the GeoMx DSP platform	0	0	10
De novo/secondary/therapy-related	244/46/0	36/4/0	39/5/2
Response to induction chemotherapy			
Yes	210	26 (M1*)	33
No	80	3 (M2*)	4
Primary induction failure	39	2	2
N.A.	-	5	3
Relapse			
Yes	132	18	31
No	118	15	15
N.A.	1	1	0
Median follow-up time (months)	101.23	70.2	55.54
Median RFS (months)	19.1	25.6	13.64
Median OS (months)	21.37	66.8	50.58

Legend: N.A. = Not available; PMCC = Princess Margaret Cancer Centre; CHOP = Children's Hospital of Philadelphia; SAL = Studienallianz Leukämie; ELN = European Leukemia-Net; BM = bone marrow; DSP = digital spatial profiling; N.A. = not available. Median follow-up time was calculated using the reverse Kaplan-Meier method, with the event indicator reversed so that the outcome of interest becomes censored. *M1, M2 and M3 BM remission status was defined as <5%, 5% to 24% and >25% AML blasts after induction chemotherapy, respectively (*73*). RFS = relapse-free survival; OS = overall survival.
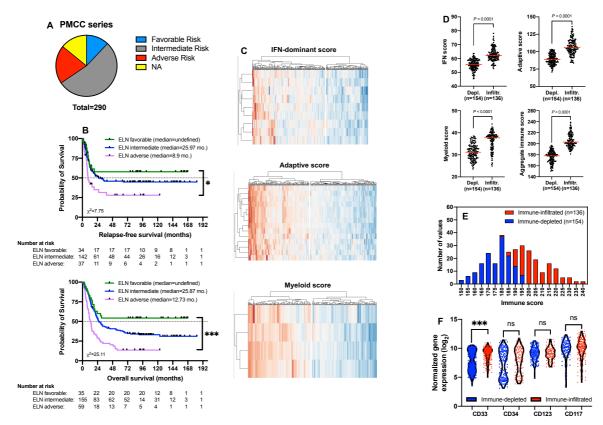
Supplementary Figures

Fig. S1: Immune gene signatures and survival in the AML discovery series. **A**) Pie chart showing patient distribution by European Leukemia Net (ELN) cytogenetic risk category in the PMCC cohort (n=290 cases). NA = not available. **B**) Cohort-wide relapse-free survival (RFS) and overall survival (OS); disease and patient characteristics are detailed in **Table 1**. The Kaplan-Meier method was used to generate survival curves, which were compared using a log-rank test (*p<0.05; ***p<0.001). Tick marks indicate censored observations. **C**) Interferon (IFN), adaptive, and myeloid signature scores individually separate AML cases according to high and low expression values. ClustVis, an online tool for clustering of multivariate data, was used for data analysis and visualization. **D**) Immune scores in the immune-depleted and immune-infiltrated subgroups. Data were compared using the Mann-Whitney *U* test for unpaired determinations. Red bars indicate median values. **E**) Distribution of the aggregate immune score in patients with immune-infiltrated and immune-depleted AML. **F**) Violin plots summarizing the expression of leukemia-associated markers (CD33, CD34, CD123, CD117) in immune-infiltrated and immune-depleted AML cases from the PMCC cohort. Data were compared using the Mann-Whitney *U* test for unpaired determinations (*p<0.05; ***p<0.001; ns=not significant). **E**) Kaplan-Meier estimate of RFS in patients with AML separated by immune gene score quartiles (highest [n=78] and lowest [n=79]). Survival curves were compared using the log-rank test (*p<0.05; **p<0.01).
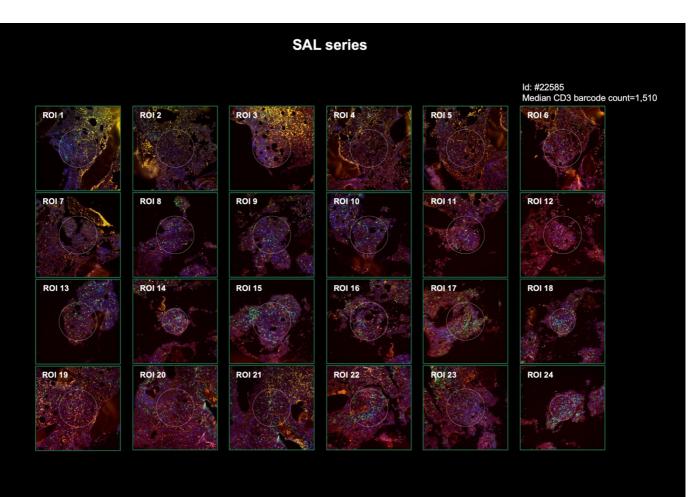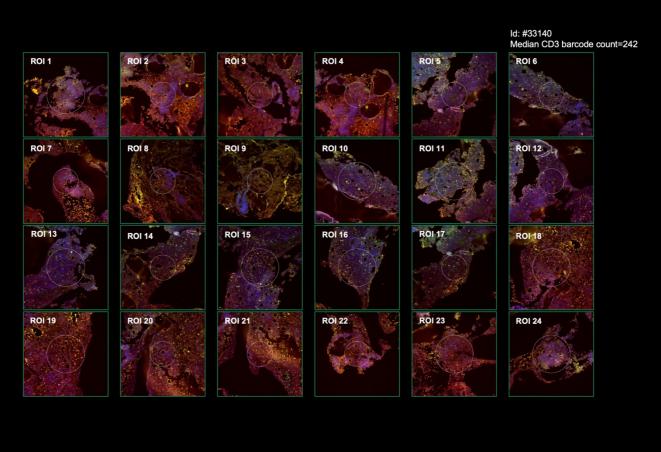
Fig. S2: GeoMx digital spatial profiling (DSP) and region of interest (ROI) selection in a representative pre-treatment BM trephine biopsy (SAL series) with high T-cell infiltration. CD3 staining is shown in green. The median CD3 barcode count (24 ROIs) is indicated.
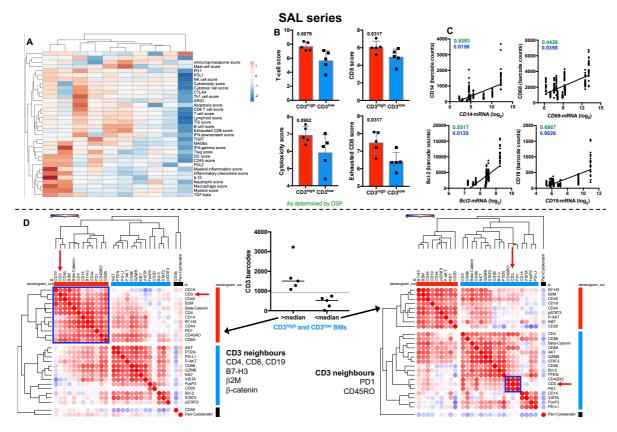
Fig. S3: GeoMx digital spatial profiling (DSP) and region of interest (ROI) selection in a representative pre-treatment BM trephine biopsy (SAL series) with low T-cell infiltration. CD3 staining is shown in green. The median CD3 barcode count (24 ROIs) is indicated.

Fig. S4: Highly multiplexed protein profiling in the SAL patient cohort. A) Unsupervised hierarchical clustering (Euclidean distance, complete linkage) of immune cell type-specific and biological activity scores (mRNA measurements using the PanCancer Immune Profiling panel) in 10 pre-treatment BM trephine biopsies used for GeoMx DSP. ClustVis, an online tool for clustering of multivariate data, was used for data analysis and visualization. **B)** Association between CD3 protein expression, as determined by GeoMx DSP, and mRNA immune gene signatures (T-cell score, CD8 score, exhausted CD8 score, NK score, cytotoxicity score and macrophage score) as measured with the nCounter platform. Data were compared using the Mann-Whitney U test for unpaired determinations. **C)** Correlation between mRNA and protein expression, as determined by GeoMx DSP. Spearman rank correlation coefficients are shown in green; *p* values are shown in blue. **D)** Unsupervised hierarchical clustering (Euclidean distance, complete linkage) of the correlation matrix of immuno-oncology proteins detected with GeoMx Digital Spatial Profiling (DSP) allows the identification of CD3 neighbors in 10 pre-treatment BM trephine biopsies from adult patients with high and low T-cell infiltration (median split). β2M=β2-microglobulin. Morpheus, an online tool developed at the Broad Institute (MA, USA) was used for data analysis and visualization.
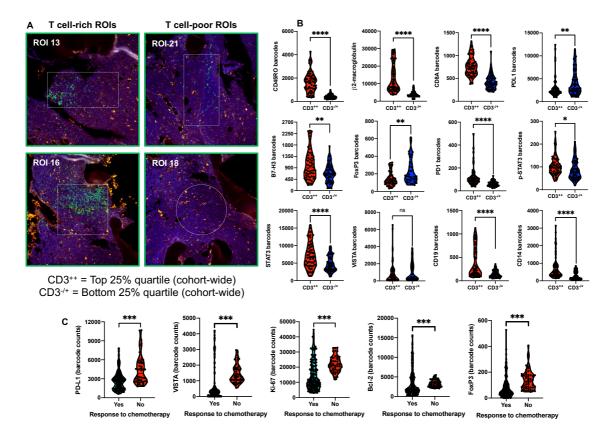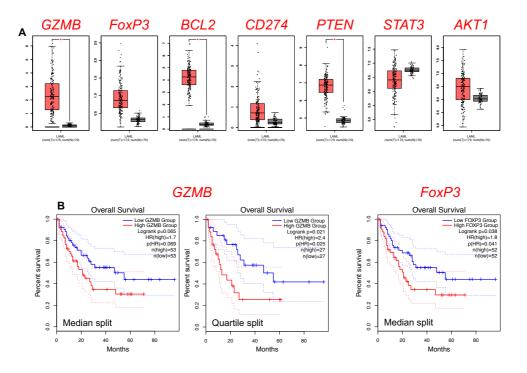
Fig. S5: Correlation between CD3 infiltration and expression of immuno-oncology (IO)-related proteins as revealed by GeoMx digital spatial profiling (DSP) of BM trephine biopsies (SAL series). A) CD3 staining is shown in green. ROIs (n=24) were assigned to either the T-cell-rich (CD3 "hotspot"; top 25% quartile of CD3 barcode counts) or the T-cell-poor category (bottom 25% quartile of CD3 barcode counts). **B**) Violin plots showing expression of CD8, β2-microglobulin, activation marker CD45RO, B7-H3, PD1, total and phosphorylated STAT3, CD14 and CD19 in relation to CD3 infiltration. Data were compared using the Mann-Whitney U test for unpaired determinations (*P<0.05; **P<0.01; ****P<0.0001; ns=not significant). **C**) Violin plots showing the association between protein expression and response to induction chemotherapy, which was defined as either morphologic complete remission (CR) or early blast clearance (<10% blasts on day 16, i.e., one week after the end of induction chemotherapy), as previously published (*45, 74*). Data were compared using the Mann-Whitney U test for unpaired determinations (***P<0.001).

Fig. S6: Expression of SIG3 genes in TCGA-AML cases and in healthy tissues. **A**) Comparison of SIG3 gene expression in TCGA-AML cases (n=173) and in normal blood (n=70; Genotype Tissue Expression [GTEx] samples). Data were accessed and analyzed using GEPIA2 (http://gepia2.cancer-pku.cn/#index). **B**) *GZMB* and *FoxP3* survival predictions. A median split and/or quartile split of gene expression scores was used to compute Kaplan-Meier curves.
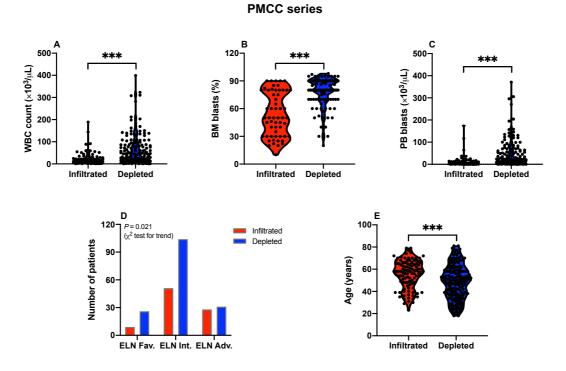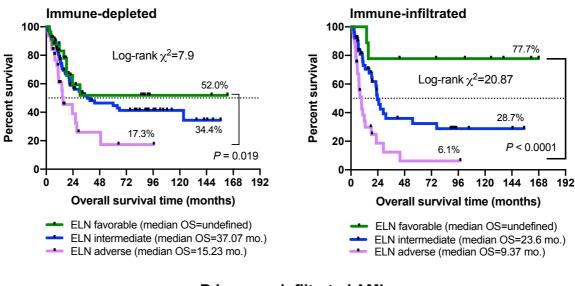
PMCC series

Fig. S7: Association between immune gene signatures and patients' characteristics in the AML discovery series. Violin plots summarizing white blood cell (WBC) count (**A**), percentage of bone marrow (BM) blasts (**B**) and peripheral blood (PB) blasts (**C**), ELN cytogenetic risk category (**D**) and age at diagnosis (**E**) in immune-infiltrated and immune-depleted patients (PMCC cohort; n=290 cases). Immune gene signatures were derived as detailed in **Fig. 1**. Comparisons were performed using the Mann-Whitney *U* test for unpaired determinations. *P<0.05; ***P<0.001.

PMCC series

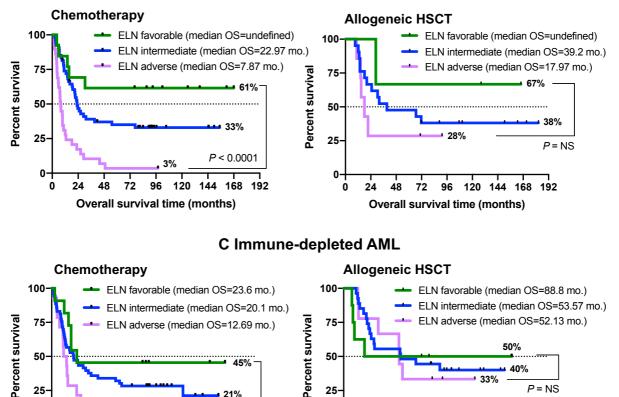## A Censored on the date of allogeneic HSCT

Immune-depleted

Log-rank χ^2=7.9

52.0%

34.4%

17.3%

P = 0.019

ELN favorable (median OS=undefined)
ELN intermediate (median OS=37.07 mo.)
ELN adverse (median OS=15.23 mo.)

Immune-infiltrated

77.7%

Log-rank χ^2=20.87

28.7%

6.1%

P < 0.0001

ELN favorable (median OS=undefined)
ELN intermediate (median OS=23.6 mo.)
ELN adverse (median OS=9.37 mo.)

B Immune-infiltrated AML

Chemotherapy

ELN favorable (median OS=undefined)
ELN intermediate (median OS=22.97 mo.)
ELN adverse (median OS=7.87 mo.)

61%

33%

3%

P < 0.0001

Allogeneic HSCT

ELN favorable (median OS=undefined)
ELN intermediate (median OS=39.2 mo.)
ELN adverse (median OS=17.97 mo.)

67%

38%

28%

P = NS

C Immune-depleted AML

Chemotherapy

ELN favorable (median OS=23.6 mo.)
ELN intermediate (median OS=20.1 mo.)
ELN adverse (median OS=12.69 mo.)

45%

21%

14%

P = 0.041

Allogeneic HSCT

ELN favorable (median OS=88.8 mo.)
ELN intermediate (median OS=53.57 mo.)
ELN adverse (median OS=52.13 mo.)

50%

40%

33%

P = NS

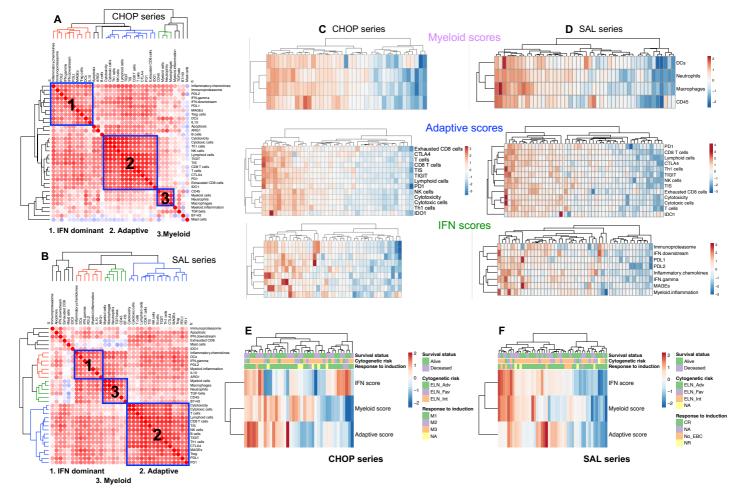**Fig. S8**: **Clinical outcomes of patients with immune-infiltrated and immune-depleted AML treated with allogeneic HSCT (PMCC cohort)**. **A**) Kaplan-Meier estimate of overall

survival (OS) in patients with immune-infiltrated and immune-depleted AML censored on the date of allogeneic HSCT. Survival curves were compared using a log-rank (Mantel-Cox) test. **B**) Kaplan-Meier estimate of overall survival (OS) in patients with immune-infiltrated AML treated with chemotherapy either alone or in combination with allogeneic HSCT. Patients were stratified based on ELN risk. Survival curves were compared using a log-rank (Mantel-Cox) test. **C**) Kaplan-Meier estimate of overall survival in patients with immune-depleted AML treated with chemotherapy either alone or in combination with allogeneic HSCT. Patients were stratified based on ELN risk. Survival curves were compared using a log-rank (Mantel-Cox) test.

Fig. S9: Immune gene signatures in the CHOP and SAL cohorts. A-B) Unsupervised hierarchical clustering (Euclidean distance, complete linkage) of the correlation matrix of immune and biological activity signatures highlights co-expression patterns of immune gene sets (Pearson correlation coefficient >0.45; blue boxes) in diagnostic bone marrow (BM) samples from children (CHOP cohort; n=34) and adults with AML (SAL cohort; n=46), namely, IFN-dominant signatures, adaptive immunity signatures and myeloid signatures. Morpheus was used for data analysis and visualization. **C-D**) Gene signatures in the IFN, adaptive, and myeloid scores stratify children and adults with AML (CHOP and SAL series) into subgroups with high and low expression. ClustVis was used for data analysis and visualization. **E-F**) IFN, adaptive, and myeloid scores in aggregate stratify children and adults with AML (CHOP and SAL series) into immune-infiltrated and immune-depleted subgroups. ClustVis was used for data analysis and visualization. ELN = 2017 European Leukemia-Net. Criteria for response to induction chemotherapy (M1 through M3 in the top panel and early blast clearance [EBC]/complete remission [CR] in the bottom panel) are detailed in **Table 1**. ADV=adverse; INT=intermediate; FAV=favorable; NA=not available; NR=no response.
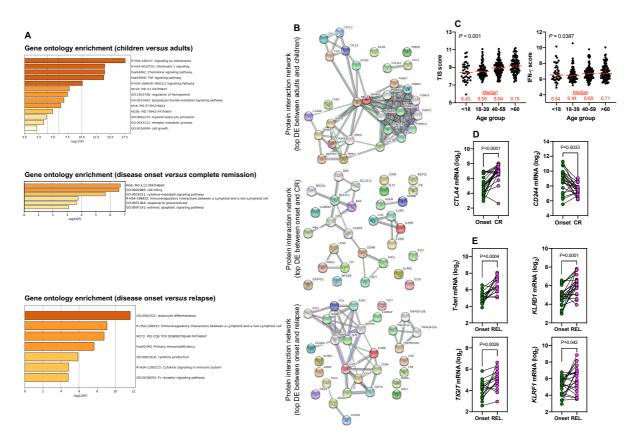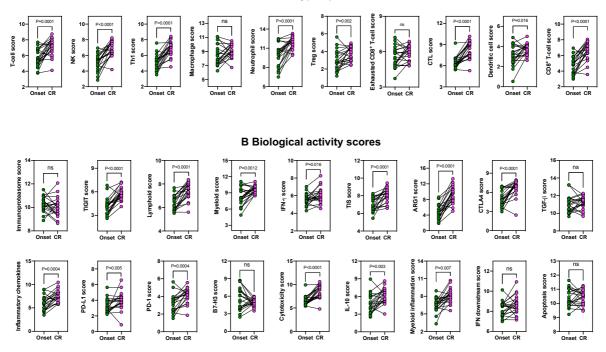
Fig. S10: Gene ontology and pathway analyses. **A**) Gene Ontology (GO) enrichment analysis. For each given gene list submitted to metascape.org, pathway and process enrichment analyses were carried out using all genes in the genome as the enrichment background. Terms with a *p* value <0.01, a minimum count of 3, and an enrichment factor >1.5 (defined as the ratio between the observed counts and the counts expected by chance) were collected and grouped into clusters based on their membership similarities. **B**) The Search Tool for the Retrieval of Interacting Genes/Proteins (STRING) database (http://string-db.org) was used to critically assess and integrate protein-protein interactions between the top 20 genes differentially expressed in adults and children with AML, as well as across disease stages (diagnosis, achievement of complete remission [CR], relapse). A detailed list of significantly enriched GO processes and KEGG pathways ranked by false discovery rate (<1×10^{-7}) is provided as **tables S4-S6**. Protein network analysis and predicted functional partners of differentially expressed (DE) genes with the highest-confidence interaction scores (>0.900) are shown. Network nodes (query proteins) represent proteins produced by a single, protein-coding gene locus. White nodes represent second shells of interactors. Empty and filled nodes indicate proteins of unknown or partly known 3D structure, respectively. Edges represent protein-protein associations. Line shapes denote predicted modes of action. **C**) Tumor inflammation signature (TIS) and IFN-γ scores across age groups. Data were compared using the Kruskal-Wallis test for unpaired determinations. **D**) Expression of select immune checkpoints and co-inhibitory molecules between matched BM samples from adult

patients (SAL series) at disease onset and complete remission (CR; n=22). **E**) Expression of genes associated with T-cell senescence/terminal differentiation/exhaustion (*TIGIT*, *TBX21* or T-bet, *KLRD1* and *KLRF1*) in matched BM samples from adult patients (SAL series) at disease onset and relapse (n=22). Data were compared using the Mann-Whitney *U* test for paired determinations. **P<0.01. ns=not significant.

Fig. S11: Immune scores in AML patients (SAL cohort) at time of diagnosis and achievement of complete remission (paired samples). A) Immune cell type-specific scores in BM samples from 21 patients with AML at time of diagnosis and achievement of complete remission (CR; SAL cohort). B) Biological activity scores in BM samples from 21 patients with AML at time of diagnosis and achievement of complete remission (CR; SAL cohort). Data were compared using the Mann-Whitney *U* test for paired determinations.
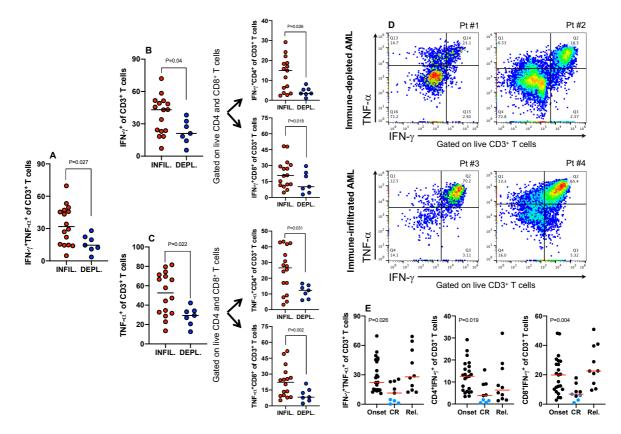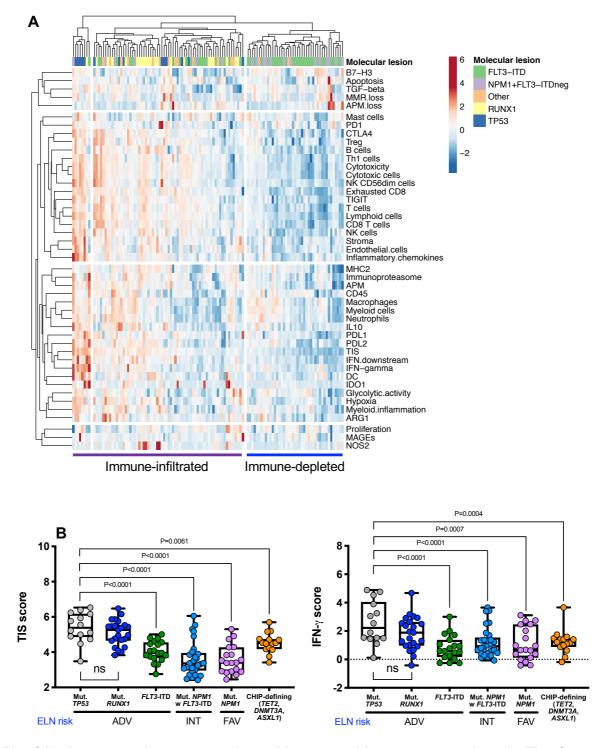
Fig. S12: Intracellular cytokine staining of BM samples from patients with immune-infiltrated and immune-depleted AML. Frequency of polyfunctional IFN-γ⁺TNF-α⁺ T cells (A), single-positive IFN-γ⁺ T cells (B) and single-positive TNF-α⁺ T cells (C) in diagnostic BM samples from patients with immune-infiltrated (n=16) and immune-depleted AML (n=7). Comparisons were performed using the Mann-Whitney *U* test for unpaired data. D) Flow cytometric analysis of intracellular cytokine production in representative BM samples from patients with immune-infiltrated (INFIL) and immune-depleted (DEPL) AML. E) Frequency of polyfunctional IFN-γ⁺TNF-α⁺ T cells and IFN-γ⁺-producing CD4⁺ and CD8⁺ T cells in diagnostic BM samples from AML patients at time of disease onset, achievement of complete remission (CR) and relapse. Data were compared using the Kruskal-Wallis test for unpaired determinations. Cases with documented minimal residual disease (MRD) negativity are shown as blue dots (immune-infiltrated subgroup).
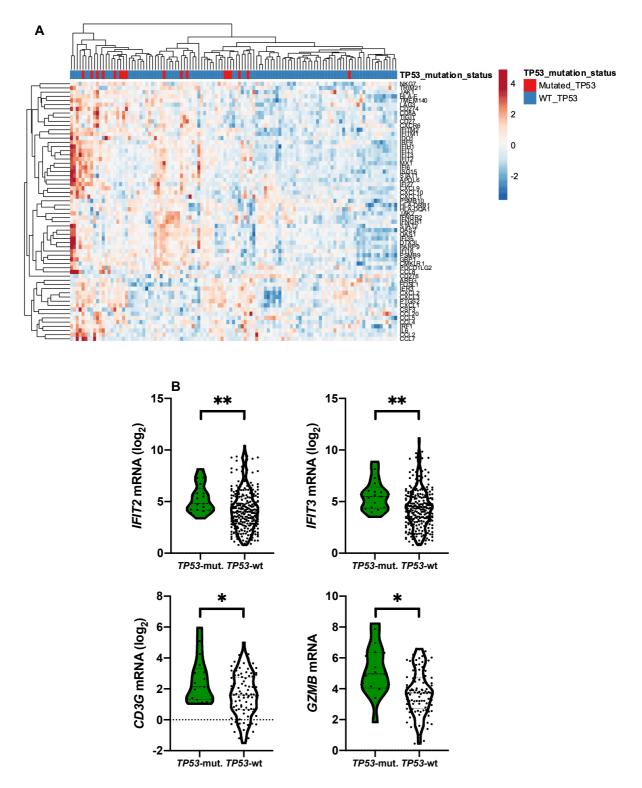
Fig. S13: Immune subtypes associate with cancer driver gene mutations in The Cancer Genome Atlas (TCGA)-AML specimens. A) Unsupervised hierarchical clustering (Euclidean distance, complete linkage) of immune cell type signatures and biological activity signatures in TCGA-AML cases stratified by prognostic molecular lesions. ClustVis was used for data analysis and visualization. B) Expression of IFN-related gene sets (as defined in **Fig. 1**) in TCGA cases with *TP53* mutations (adverse molecular risk), *NPM1* mutations without *FLT3*-ITD (ELN favorable
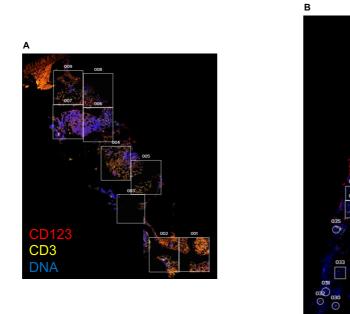
risk), FLT3-*ITD* without *NPM1* mutations (ELN adverse risk), *RUNX1* mutations (adverse molecular risk). Other = clonal hematopoiesis of indeterminate potential (CHIP)-defining mutations (*TET2*, *DNMT3A*, *ASXL1*). Comparisons were performed using the Kruskal-Wallis test for unpaired determinations.

Beat-AML series

A

B

Fig. S14: Genes implicated in IFN downstream signaling in Beat AML trial specimens with *TP53* mutations. A) Expression of IFN-downstream genes in Beat AML cases with (n=21) or without *TP53* mutations (n=128). ClustVis was used for data analysis and visualization. B) Violin plots summarizing the expression of surrogate markers of T-cell infiltration and cytotoxicity in Beat

AML cases with or without *TP53* mutations. Comparisons were performed with the Mann-Whitney *U* test for unpaired data. *P<0.05; **P<0.01.

Fig. S15: Identification of regions of interest in BM biopsies from patients receiving flotetuzumab immunotherapy. Regions of interest (ROIs) covering the entire FFPE BM biopsy were selected for highly multiplexed protein profiling on the GeoMx DSP platform. Two representative patients are shown in panels A and B.

Supplementary Tables

Supplemental Table 1. Differentially expressed (DE) genes (false discovery rate<0.05) between ELN favorable-risk and adverse-risk AML (HOVON discovery cohort).

Official symbol	Official full name	Location	NanoString probe ID	Synonyms; previous symbols
APP	Amyloid beta precursor protein	21q21.3	NM_000484.3:1725	AD1
ARG2	Arginase 2	14q24.1	NM_001172.3:1150	
CARD11	Caspase recruitment domain family member 11	7p22.2	NM_032415.2:1075	CARMA1, BIMP3
CCL23	C-C motif chemokine ligand 23	17q12	NM_145898.1:336	SCYA23, Ckb-8, MPIF-1, MIP-3, CKb8
CD34	CD34 molecule	1q32.2	NM_001025109.1:1580	
CD55	CD55 molecule	1q32.2	NM_000574.3:101	DAF, CR, TC, CROM
CT45A1	Cancer/testis antigen family 45 member A1	Xq26.3	NM_001017417.1:866	CT45-1, CT45.1
CYFIP2	Cytoplasmic FMR1 interacting protein 2	5q33.3	NM_001037332.2:4043	PIR121
DPP4	Dipeptidyl peptidase 4	2q24.2	NM_001935.3:2700	CD26, ADCP2, DPPIV
F2RL1	F2R like trypsin receptor 1	5q13.3	NM_005242.3:940	GPR11, PAR2
IL15	Interleukin 15	4q31.21	NM_172174.1:1685	IL-15, MGC9721
IL2RA	Interleukin 2 receptor subunit alpha	10p15.1	NM_000417.1:1000	IL2R, IDDM10, CD25
LILRA4	Leukocyte immunoglobulin like receptor A4	19q13.42	NM_012276.3:1577	
MAF	MAF bZIP transcription factor	16q23.2	NM_005360.4:888	c-MAF
MRC1	Mannose receptor C-type 1	10p12.33	NM_002438.2:525	MRC1L1, CLEC13D, CD206, bA541I19.1, CLEC13DL
NFATC1	Nuclear factor of activated T cells 1	18q23	NM_172389.1:1984	NF-ATC, NFATc, NFAT2
PNMA1	PNMA family member 1	14q24.3	NM_006029.4:1565	MA1
PRM1	Protamine 1	16p13.13	NM_002761.2:319	CT94.1
RAG1	Recombination activating 1	11p12	NM_000448.2:2300	RNF74, MGC43321
STAT4	Signal transducer and activator of transcription 4	2q32.2-q32.3	NM_003151.2:789	ILT7, CD85g

| *TNFRSF18* | TNF receptor superfamily member 18 | 1p36.33 | NM_004195.2:445 | AITR, GITR, CD357 |

Table S2. Competing risks analysis for overall survival (OS) prediction (PMCC discovery cohort).

	SHR	Std. Err.	z	P> /z/	95% CI
IFN score	1.053864	0.0266407	2.08	**0.038**	1.002922-1.107394
Innate score	0.9683486	0.0264452	-1.18	0.239	0.9178796-1.021593
Adaptive score	0.9996771	0.0090025	-0.04	0.971	0.9821873-1.017478

Number of observations = 249
Number failed = 125
Number competing = 75
Number censored = 49
Wald χ^2 = 6.15

Legend: SHR = Estimated subhazard ratio; Std. Err. = standard error; CI = Confidence interval; IFN = interferon.
Competing risk analyses were performed using STATA/IC (version 16.0).
HSCT, a potential confounder, was treated as an event whose occurrence precluded the occurrence of the primary clinical endpoint (death).

Table S3. Causes of death in patients receiving allogeneic hematopoietic stem cell transplantation (HSCT; PMCC cohort).

Cause of death	Immune-infiltrated (n=36)	Immune-depleted (n= 52)
Treatment-related toxicity*	3 (8%)	1 (2%)
Graft-versus-host disease	8 (22%)	8 (15%)
Leukemia recurrence	9 (25%)	11 (21%)
Infections	3 (8%)	9 (17%)
Other ; not known	0 ; 13 (36%)	4 ; 19 (44%)

*Including sinusoidal obstruction syndrome.

Table S4. Gene ontologies (GO) of and KEGG pathways captured by DE genes between adult (SAL cohort) and childhood AML (CHOP cohort).

GO term	Description	Count in gene set	FDR
GO:0002376	Immune system process	26	4.03×10^{-17}
GO:0006955	Immune response	22	1.79×10^{-15}
GO:0016579	Protein deubiquitination	13	5.31×10^{-14}
GO:0071347	Cellular response to interleukin 1	10	1.24×10^{-12}
GO:0070423	Nucleotide-binding oligomerization domain containing signaling pathway	7	1.01×10^{-11}
GO:0006508	Proteolysis	17	2.30×10^{-11}
GO:0045321	Leukocyte activation	15	9.49×10^{-11}
GO:0006950	Response to stress	23	1.03×10^{-10}
GO:0050896	Response to stimulus	30	1.33×10^{-10}
GO:0070498	Interleukin 1-mediated signaling pathway	7	2.76×10^{-10}
GO:0006954	Inflammatory response	12	3.22×10^{-10}
GO:0002758	Innate immune response-activating signal transduction	9	3.62×10^{-10}
GO:0002221	Pattern recognition receptor signaling pathway	8	7.58×10^{-10}
GO:0051603	Proteolysis involved in cellular protein catabolic process	12	7.58×10^{-10}
GO:0070647	Protein modification by small protein conjugation or removal	14	1.91×10^{-9}
GO:0006511	Ubiquitin-dependent protein catabolic process	11	3.24×10^{-9}
GO:0034097	Response to cytokine	14	5.12×10^{-9}
GO:0010033	Response to organic substance	20	5.49×10^{-9}
GO:0019221	Cytokine-mediated signaling pathway	12	6.08×10^{-9}
Pathway ID	**Description**	**Count in gene set**	**FDR**
hsa05169	Epstein-Barr virus infection	17	1.92×10^{-24}
hsa03050	Proteasome	10	1.21×10^{-17}
hsa04620	Toll-like receptor signaling pathway	10	2.03×10^{-14}
hsa05142	Chagas disease (American trypanosomiasis)	10	2.03×10^{-14}
hsa04657	IL-17 signaling pathway	9	4.62×10^{-13}
hsa04621	NOD-like receptor signaling pathway	10	1.12×10^{-12}
hsa04668	TNF signaling pathway	9	1.28×10^{-12}
hsa04062	Chemokine signaling pathway	10	1.92×10^{-12}
hsa05167	Kaposi's sarcoma-associated herpesvirus infection	10	1.92×10^{-12}
hsa04064	NF-kappa B signaling pathway	8	1.98×10^{-11}
hsa04622	RIG-I-like receptor signaling pathway	7	1.86×10^{-10}
hsa05161	Hepatitis B	8	4.09×10^{-10}
hsa05134	Legionellosis	6	2.72×10^{-9}
hsa05131	Shigellosis	6	5.99×10^{-9}
hsa05120	Epithelial cell signaling in Helicobacter pylori infection	6	7.27×10^{-9}
hsa05132	Salmonella infection	6	2.66×10^{-8}

hsa05168	Herpes simplex infection	7	$6.58×10^{-8}$
hsa05145	Toxoplasmosis	6	$1.04×10^{-7}$
hsa04380	Osteoclast differentiation	6	$2.06×10^{-7}$
hsa05160	Hepatitis C	6	$2.68×10^{-7}$

Table S5. GO of and KEGG pathways captured by DE genes between adult AML patients at the time of diagnosis and achievement of complete remission (SAL cohort).

GO term	Description	Count in gene set	FDR
GO:0002376	Immune system process	20	$7.85×10^{-9}$
GO:0046902	Regulation of mitochondrial membrane permeability	7	$2.04×10^{-8}$
GO:0052150	Modulation by symbiont of host apoptotic process	4	$2.49×10^{-7}$
GO:1902533	Positive regulation of intracellular signal transduction	13	$2.49×10^{-7}$
GO:0006955	Immune response	15	$2.58×10^{-7}$
GO:0007166	Cell surface receptor signaling pathway	17	$2.58×10^{-7}$
GO:0019221	Cytokine-mediated signaling pathway	11	$2.58×10^{-7}$
GO:0031341	Regulation of cell killing	6	$2.58×10^{-7}$
GO:0034097	Response to cytokine	13	$2.58×10^{-7}$
GO:0071310	Cellular response to organic substance	17	$2.60×10^{-7}$
GO:0010821	Regulation of mitochondrion organization	7	$2.95×10^{-7}$
GO:1901030	Positive regulation of mitochondrial outer membrane permeabilization involved in apoptotic signaling pathway	5	$3.11×10^{-7}$
GO:0048583	Regulation of response to stimulus	21	$3.59×10^{-7}$
GO:0070887	Cellular response to chemical stimulus	18	$4.02×10^{-7}$
GO:0044419	Interspecies interaction between organisms	11	$4.46×10^{-7}$
GO:0010822	Positive regulation of mitochondrion organization	6	$4.67×10^{-7}$
GO:0071345	Cellular response to cytokine stimulus	12	$5.40×10^{-7}$
GO:0048584	Positive regulation of response to stimulus	16	$5.56×10^{-7}$
GO:2001235	Positive regulation of apoptotic signaling pathway	7	$5.56×10^{-7}$
Pathway ID	**Description**	**Count in gene set**	**FDR**
hsa04210	Apoptosis	8	$3.58×10^{-9}$
hsa04215	Apoptosis - multiple species	5	$1.14×10^{-7}$
hsa05200	Pathways in cancer	10	$1.15×10^{-7}$
hsa01524	Platinum drug resistance	5	$2.51×10^{-6}$
hsa05202	Transcriptional mis-regulation in cancer	6	$4.90×10^{-6}$
hsa04151	PI3K-Akt signaling pathway	7	$1.52×10^{-5}$
hsa05014	Amyotrophic lateral sclerosis (ALS)	4	$2.03×10^{-5}$
hsa05166	HTLV-I infection	6	$2.84×10^{-5}$
hsa04060	Cytokine-cytokine receptor interaction	6	$3.36×10^{-5}$
hsa05212	Pancreatic cancer	4	$6.24×10^{-5}$
hsa05220	Chronic myeloid leukemia	4	$6.27×10^{-5}$
hsa01521	EGFR tyrosine kinase inhibitor resistance	4	$6.35×10^{-5}$
hsa05210	Colorectal cancer	4	$8.12×10^{-5}$
hsa05340	Primary immunodeficiency	3	0.00023
hsa05161	Hepatitis B	4	0.00049

hsa04630	JAK-STAT signaling pathway	4	0.00072
hsa05213	Endometrial cancer	3	0.00072
hsa05225	Hepatocellular carcinoma	4	0.00072
hsa04137	Mitophagy - animal	3	0.00077
hsa05223	Non-small cell lung cancer	3	0.00084

Table S6. GO of and KEGG pathways captured by DE genes between adult AML patients at the time of relapse and achievement of complete remission (SAL cohort).

GO term	Description	Count in gene set	FDR
GO:0007166	Cell surface receptor signaling pathway	23	$1.96×10^{-13}$
GO:0002376	Immune system process	21	$1.90×10^{-10}$
GO:0034097	Response to cytokine	16	$1.90×10^{-10}$
GO:0006955	Immune response	18	$2.07×10^{-10}$
GO:0007165	Signal transduction	26	$2.56×10^{-10}$
GO:0051716	Cellular response to stimulus	28	$5.39×10^{-10}$
GO:0071345	Cellular response to cytokine stimulus	14	$4.73×10^{-9}$
GO:0050896	Response to stimulus	29	$7.20×10^{-9}$
GO:0010033	Response to organic substance	20	$1.27×10^{-9}$
GO:0019221	Cytokine-mediated signaling pathway	12	$1.27×10^{-9}$
GO:0071310	Cellular response to organic substance	18	$2.31×10^{-9}$
GO:0010941	Regulation of cell death	16	$2.72×10^{-9}$
GO:0002521	Leukocyte differentiation	9	$7.30×10^{-9}$
GO:0009612	Response to mechanical stimulus	8	$8.11×10^{-9}$
GO:0030217	T cell differentiation	7	$1.02×10^{-7}$
GO:0010942	Positive regulation of cell death	11	$1.63×10^{-7}$
GO:0050776	Regulation of immune response	12	$1.90×10^{-7}$
GO:0002682	Regulation of immune system process	14	$2.88×10^{-7}$
GO:0002768	Immune response-regulating cell surface receptor signaling pathway	8	$3.57×10^{-7}$
Pathway ID	**Description**	**Count in gene set**	**FDR**
hsa04659	Th17 cell differentiation	9	$5.81×10^{-12}$
hsa04658	Th1 and Th2 cell differentiation	8	$6.86×10^{-11}$
hsa04660	T cell receptor signaling pathway	8	$1.11×10^{-10}$
hsa04210	Apoptosis	8	$8.77×10^{-10}$
hsa04060	Cytokine-cytokine receptor interaction	9	$3.86×10^{-9}$
hsa04380	Osteoclast differentiation	7	$1.58×10^{-8}$
hsa04650	Natural killer cell mediated cytotoxicity	7	$1.58×10^{-8}$
hsa05164	Influenza A	7	$8.94×10^{-8}$
hsa04217	Necroptosis	6	$1.63×10^{-6}$
hsa05210	Colorectal cancer	5	$2.47×10^{-6}$
hsa04657	IL-17 signaling pathway	5	$3.27×10^{-6}$
hsa05142	Chagas disease (American trypanosomiasis)	5	$4.67×10^{-6}$
hsa04668	TNF signaling pathway	5	$5.93×10^{-6}$
hsa05162	Measles	5	$1.48×10^{-5}$
hsa05166	HTLV-I infection	6	$1.48×10^{-5}$
hsa05120	Epithelial cell signaling in Helicobacter pylori infection	4	$2.48×10^{-5}$
hsa04010	MAPK signaling pathway	6	$3.20×10^{-5}$
hsa05133	Pertussis	4	$3.40×10^{-5}$
hsa05132	Salmonella infection	4	$5.21×10^{-5}$
hsa01522	Endocrine resistance	4	$7.90×10^{-5}$

Table S7: Binary logistic regression predicting therapeutic resistance (PMCC cohort).

Model 1	B	Wald $\chi 2$	*p*	OR
ELN risk category		28.64	0	
Favorable vs. adverse	-2.97	14.77	0	0.05
Intermediate vs. adverse	-1.52	21.36	0	0.22
Model $\chi 2$	33.43			
P value	0			
-2LL	254.6			
Nagelkerke (pseudo R2)	0.183			
Sensitivity	48.0%			
Specificity	85.2%			
False positive rate	45.8%			
False negative rate	17.9%			
AUROC	0.702			

Model 2	B	Wald $\chi 2$	*p*	OR
ELN risk category		29.63	0	
Favorable vs. adverse	-3.001	15.1	0	0.05
Intermediate vs. adverse	-1.613	22.37	0	0.2
WBC	0.003	1.44	0.23	1.003
Model $\chi 2$	34.82			
P value	0			
-2LL	253.2			
Nagelkerke (pseudo R2)	0.190			
Sensitivity	50.0%			
Specificity	85.2%			
False positive rate	45.0%			
False negative rate	17.5%			
AUROC	0.731			

Model 3	B	Wald $\chi 2$	*p*	OR
ELN risk category		28.51	0	
Favorable vs. adverse	-3.005	14.88	0	0.05
Intermediate vs. adverse	-1.583	21.29	0	0.22
WBC	0.004	1.84	0.175	1.004
AML type (primary *versus* secondary)	-0.65	2.59	0.108	0.52
Model $\chi 2$	37.33			
P value	0			
-2LL	250.6			
Nagelkerke (pseudo R2)	0.203			
Sensitivity	50.0%			
Specificity	85.2%			
False positive rate	45.0%			
False negative rate	17.5%			
AUROC	0.731			

Model 4	B	Wald $\chi 2$	*p*	OR

	B	Wald χ^2	p	OR
ELN risk category		28.35	0	
Favorable vs. adverse	-3.07	15.37	0	0.05
Intermediate vs. adverse	-1.56	20.57	0	0.21
WBC	0.003	1.54	0.215	1.003
AML type (primary *versus* secondary)	-0.78	3.371	0.066	0.457
Age	-0.012	1.111	0.292	0.989
Model χ^2	38.45			
P value	0			
-2LL	249.5			
Nagelkerke (pseudo R2)	0.318			
Sensitivity	50.0%			
Specificity	85.2%			
False positive rate	46.0%			
False negative rate	17.5%			
AUROC	0.775			
Model 5	**B**	**Wald χ^2**	***p***	**OR**
ELN risk category		27.38	0	
Favorable vs. adverse	-3.63	18.83	0	0.03
Intermediate vs. adverse	-1.65	16.9	0	6
WBC	0.006	3.83	**0.05**	1.003
AML type (primary *versus* secondary)	-0.49	0.84	0.36	0.65
Age	-0.02	1.36	0.244	0.985
Myeloid inflammation	0.6	9.06	**0.003**	1.822
Inflammatory chemokines	-0.37	1.99	0.16	0.69
IFN-γ	-0.82	6.07	**0.014**	0.439
IFN downstream	0.87	4.49	**0.034**	2.4
Immunoproteasome	0.62	1.29	0.256	1.86
IL-10	-0.17	0.58	0.45	0.85
PD-L1	-0.09	0.07	0.79	0.914
PD-L2	0.397	1.92	0.166	1.49
MAGEs	0.16	0.11	0.74	1.18
Model χ^2	65.87			
P value	0			
-2LL	222.1			
Nagelkerke (pseudo R2)	0.339			
Sensitivity	63.6%			
Specificity	88.0%			
False positive rate	34.3%			
False negative rate	13.0%			
AUROC	0.815			

Legend: Predicted likelihood of response to induction chemotherapy in AML patients from the PMCC cohort (n=249 cases). 2017 ELN cytogenetic risk, white blood cell count at diagnosis, disease type (primary *versus* secondary AML), patient age at diagnosis and immune gene signatures were selected as pre-treatment covariates.

Table S8: Multinomial logistic regression predicting therapeutic response (HOVON cohort).

Parameter estimates

		β	SE	Wald χ2	P value	HR	95% CI for HR	
							Lower	Upper
EFS	Intercept	-2.345	5.881	0.159	0.69			
	BM blasts	0	0.006	0.002	0.966	1	0.988	1.011
	Age	-0.006	0.009	0.498	0.48	0.994	0.977	1.011
	Lymphoid cells	1.487	1.48	1.01	0.315	4.425	0.243	80.533
	Myeloid cells	-0.309	0.441	0.492	0.483	0.734	0.309	1.742
	APM	-0.148	0.585	0.064	0.801	0.863	0.274	2.717
	MHC2	-0.24	0.132	3.323	0.068	0.787	0.608	1.018
	IFN-γ	0.271	0.483	0.314	0.575	1.311	0.509	3.38
	Cytotoxicity	-0.358	0.65	0.303	0.582	0.699	0.195	2.5
	Immunoproteasome	0.326	0.325	1.011	0.315	1.386	0.733	2.619
	Apoptosis	-0.132	0.261	0.254	0.614	0.877	0.525	1.463
	Inflamm. chemokines	0.246	0.319	0.596	0.44	1.279	0.685	2.389
	MAGEs	-3.168	1.014	9.76	**0.002**	0.042	0.006	0.307
	IFN downstream	-1.159	0.362	10.255	**0.001**	0.314	0.154	0.638
	Myeloid inflammation	-0.047	0.183	0.067	0.795	0.954	0.667	1.364
	B cells	0.114	0.389	0.085	0.77	1.12	0.522	2.403
	CD45	-0.068	0.293	0.054	0.817	0.934	0.526	1.659
	CD8$^+$ cells	-0.295	0.437	0.454	0.501	0.745	0.316	1.755
	CTLs	0.505	0.852	0.351	0.554	1.657	0.312	8.805
	DCs	1.574	0.831	3.589	0.058	4.827	0.947	24.601
	Exhausted CD8$^+$ cells	-0.487	0.497	0.96	0.327	0.614	0.232	1.628
	Macrophages	0.222	0.295	0.57	0.45	1.249	0.701	2.225
	Mast cells	0.066	0.123	0.292	0.589	1.069	0.84	1.359
	PMN	0.004	0.176	0	0.984	1.004	0.711	1.417
	NK cells	-0.462	0.523	0.782	0.377	0.63	0.226	1.755
	T cells	-0.279	0.471	0.352	0.553	0.756	0.301	1.902
	Th1	-0.004	0.478	0	0.993	0.996	0.39	2.541
	TIS	1.728	0.982	3.1	0.078	5.63	0.822	38.548
	[ELN=ADV]	0.039	0.365	0.012	0.914	1.04	0.509	2.127
	[ELN=FAV]	1.492	0.287	26.969	0	4.445	2.531	7.804
	[ELN=INT]	0^	.	.	.	.	.	.
NR	Intercept	-18.35	6.566	7.808	0.005			
	BM blasts	0.001	0.006	0.05	0.823	1.001	0.989	1.014
	Age	0.02	0.01	4.354	**0.037**	1.02	1.001	1.04
	Lymphoid cells	1.185	1.557	0.579	0.447	3.271	0.155	69.157
	Myeloid cells	0.262	0.481	0.297	0.586	1.3	0.506	3.338
	APM	0.129	0.629	0.042	0.838	1.138	0.331	3.905
	MHC2	-0.158	0.139	1.286	0.257	0.854	0.65	1.122
	IFN-γ	-0.562	0.553	1.034	0.309	0.57	0.193	1.685
	Cytotoxicity	-0.4	0.715	0.313	0.576	0.67	0.165	2.721
	Immunoproteasome	0.764	0.358	4.55	**0.033**	2.148	1.064	4.335
	Apoptosis	0.135	0.289	0.219	0.64	1.145	0.65	2.016
	Inflamm. chemokines	0.053	0.336	0.025	0.874	1.055	0.546	2.036
	MAGEs	-2.088	1.022	4.172	**0.041**	0.124	0.017	0.919
	IFN downstream	-0.437	0.368	1.414	0.234	0.646	0.314	1.328
	Myeloid inflammation	0.337	0.183	3.417	0.065	1.401	0.98	2.004

	B	SE	Wald	df	Sig	Exp(B)	Lower	Upper
B cells	0.081	0.41	0.039		0.844	1.084	0.485	2.422
CD45	0.121	0.312	0.149		0.699	1.128	0.612	2.081
CD8+ cells	-0.522	0.47	1.234		0.267	0.593	0.236	1.491
CTLs	0.439	0.919	0.228		0.633	1.551	0.256	9.384
DCs	1.651	0.873	3.579		0.059	5.215	0.942	28.861
Exhausted CD8+ cells	0.456	0.528	0.744		0.388	1.578	0.56	4.443
Macrophages	-0.176	0.335	0.277		0.599	0.838	0.435	1.616
Mast cells	0.328	0.131	6.279		**0.012**	1.389	1.074	1.795
PMN	-0.156	0.197	0.623		0.43	0.856	0.581	1.26
NK cells	-0.164	0.532	0.096		0.757	0.848	0.299	2.406
T cells	-0.275	0.497	0.308		0.579	0.759	0.287	2.009
Th1	0.018	0.476	0.001		0.97	1.018	0.401	2.587
TIS	0.331	1.034	0.102		0.749	1.392	0.183	10.563
[ELN=ADV]	1.168	0.3	15.151		**0**	3.217	1.786	5.794
[ELN=FAV]	-0.619	0.362	2.917		**0.088**	0.539	0.265	1.096
[ELN=INT]	0^	.	.		.	.	.	.
NRM Intercept	11.659	7.472	2.435	1	0.119			
BM blasts	-0.009	0.008	1.303	1	0.254	0.991	0.977	1.006
Age	0.019	0.011	2.811	1	0.094	1.019	0.997	1.042
Lymphoid cells	0.937	1.812	0.267	1	0.605	2.551	0.073	88.87
Myeloid cells	-0.233	0.561	0.173	1	0.677	0.792	0.264	2.377
APM	-1.241	0.726	2.922	1	0.087	0.289	0.07	1.199
MHC2	0.118	0.179	0.435	1	0.509	1.126	0.792	1.6
IFN-γ	-1.154	0.808	2.039	1	0.153	0.315	0.065	1.537
Cytotoxicity	0.192	0.817	0.055	1	0.814	1.211	0.244	6.003
Immunoproteasome	0.216	0.412	0.276	1	0.6	1.241	0.554	2.782
Apoptosis	-0.176	0.327	0.291	1	0.589	0.838	0.442	1.59
Inflamm. chemokines	0.401	0.407	0.972	1	0.324	1.493	0.673	3.313
MAGEs	-1.897	1.283	2.186	1	0.139	0.15	0.012	1.855
IFN downstream	-0.852	0.482	3.123	1	0.077	0.426	0.166	1.097
Myeloid inflammation	0.051	0.228	0.05	1	0.823	1.052	0.673	1.644
B cells	0.102	0.481	0.045	1	0.833	1.107	0.431	2.843
CD45	0.141	0.387	0.132	1	0.716	1.151	0.539	2.458
CD8+ cells	-0.791	0.541	2.142	1	0.143	0.453	0.157	1.308
CTLs	-0.324	1.061	0.093	1	0.76	0.723	0.09	5.792
DCs	-0.484	1.101	0.193	1	0.66	0.616	0.071	5.336
Exhausted CD8+ cells	-0.03	0.617	0.002	1	0.961	0.97	0.289	3.254
Macrophages	0.21	0.384	0.298	1	0.585	1.233	0.581	2.617
Mast cells	-0.149	0.167	0.803	1	0.37	0.861	0.621	1.194
PMN	0.13	0.221	0.348	1	0.555	1.139	0.739	1.755
NK cells	-0.334	0.652	0.262	1	0.609	0.716	0.199	2.571
T cells	0.562	0.562	1.001	1	0.317	1.755	0.583	5.28
Th1	0.154	0.586	0.069	1	0.793	1.166	0.37	3.675
TIS	2.164	1.301	2.769	1	0.096	8.707	0.681	111.402
[ELN=ADV]	0.209	0.414	0.255	1	0.614	1.232	0.548	2.773
[ELN=FAV]	0.661	0.36	3.366	1	0.067	1.937	0.956	3.924
[ELN=INT]	0^	.	.	0	.	.	.	.

* The reference category is: Relapse.
^ This parameter is set to 0 because it is redundant.

Legend: ELN cytogenetic risk, patient age, leukemia burden at diagnosis and immune gene signatures were selected as covariates (HOVON validation cohort; n=618 cases). HR = hazard ratio; DF = degrees of freedom; EFS = event-free survival; NR = no response to induction chemotherapy; NRM = non-relapse mortality; BM = bone marrow; TIS = tumor inflammation signature; MAGE = melanoma-associated antigen; IFN = interferon; PMN = polymorphonuclear cells; DC = dendritic cell; CTL = cytotoxic T lymphocyte; APM = antigen processing machinery; ELN = European Leukemia-Net; ADV = adverse cytogenetic risk; FAV = favorable cytogenetic risk; INT = intermediate cytogenetic risk.

Table S9: Study participants in the CP-MGD006-01 clinical trial (NCT#02152956) of flotetuzumab immunotherapy.

Number of patients	30
Number of BM samples	49
Baseline	30
End of cycle 1	19
Males/females (n)	14/16
Median age (range)	57 (27-74)
Age (years)	
18-65	23
66-75	7
Disease status at time of enrollment	
Relapsed AML	7
Chemotherapy-refractory AML	23
Secondary AML	12
Cytogenetic risk group (ELN; n)	
Favorable	6
Intermediate	6
Adverse	17
Unknown	1
Prior lines of therapy (n and range)	4 (1-9)
Response	
CR/CRh/CRi	8
PR	1
OB	3
TF/SD/PD	18

Legend: ELN = European Leukemia Net; CR = complete remission; CRi= CR with incomplete hematologic recovery; CRh = CR with partial hematologic recovery; OB = other benefit; TF = treatment failure; SD = stable disease; PD = progressive disease; BM = bone marrow; N.A. = not available.

Table S10: Protein panel used for GeoMx Digital Spatial Profiling (DSP) of FFPE bone marrow biopsies (SAL cohort [A] and flotetuzumab cohort [B]).

Panel A	
Housekeeping proteins	RPS6
	Histone H3
Signal-to-noise ratio	Mouse IgG control
	IgG rabbit isotype control
NK cells	CD56
	GZMB
T cells	CD3
	CD4
	CD8A
	CD45RO
	FoxP3
B cells	CD19
	CD20
Monocytes/macrophages	CD14
	CD68
Immune checkpoints	B7-H3 (CD276)
	VISTA (PD-1H)
	PD1 (CD279)
	PD-L1 (CD274)
Signaling pathways	STAT3
	P-STAT3
	AKT
	P-AKT
Cancer drivers	Bcl-2
	PTEN
	β-catenin
Other molecules	Ki-67
	CD44
	CD45
	Pan-cytokeratin
	β2-microglobulin

Panel B	
Housekeeping proteins	RPS6
	Histone H3
	GAPDH
Isotype controls	Mouse IgG1
	Rabbit IgG1
	Mouse IgG2A
Immune cell profiling core	β2-microglobulin
	CD11c
	CD20
	CD3
	CD4

	CD45
	CD56
	CD68
	CD8
	CTLA4
	GZMB
	Ki-67
	PD1 (CD279)
	PD-L1 (CD274)
	Pan-cytokeratin
	HLA-DR
	SMA
	Fibronectin
IO drug target module	4-1BB (CD137)
	LAG3
	OX40L
	Tim-3
	VISTA (PD-1H)
	ARG1
	B7-H3 (CD276)
	IDO1
	STING
	GITR
	4-1BB (CD137)
Immune activation status module	CD127
	CD25
	CD80
	ICOS
	PD-L2
	CD40
	CD27
	CD44
	CD127
Immune cell typing module	CD45RO
	FoxP3
	CD34
	CD66b
	CD14
	FAP-α
	CD163
	CD45RO
Pan-tumor module	MART1
	NY-ESO-1
	S100B
	Bcl-2
	EpCAM
	Her2/ErbB2
	PTEN
	PR

Table S11: Antibody panel used for intracellular cytokine staining of bone marrow cell suspensions.

Antigen	Clone	Fluorochrome
Surface staining		
CD3	UCHT1	PE-Dazzle 594
CD4	RPA-T4	Brilliant Violet 421
CD8	RPA-T8	APC-Fire 750
Intracellular staining		
IL-2	MQ1-17H12	FITC
IL-4	8D4-8	PE
IL-10	JES3-9D7	Alexa Fluor 647
IL-17	BL168	Per-CP-Cy5.5
TNF-	MAb11	PE-Cy7
IFN-	B27	Alexa Fluor 700